Final Technical Report for MRERP Project G09AP00041

Award number: G09AP00041

Principal investigator: Robert J. Bodnar

Title of the report: Age and petrogenesis of host rocks at the Coles Hill uranium deposit, Pittsylvania County, Virginia, USA, based on zircon U-Pb geochronology

The original proposal was to develop a genetic model for the Coles Hill uranium deposit in Pittsylvania County Virginia. The plan was to conduct a detailed geochronological and geochemical study of the host rocks and other lithologies associated with mineralization to constrain the timing of ore formation and the source of the uranium. Owing to the reduced amount of funding provided, it was decided to focus our efforts on constraining the age of the host rocks to confirm that they were part of the Martinsville Igneous Complex. This has been done and the results have been presented at the Geological Society of America meetings in 2010 and 2011. A manuscript describing the results has undergone the first round of reviews by Economic Geology and is currently under revision for re-submission – a copy is attached.

In addition to the manuscript that is currently under review, the following abstracts related to this project have been published.

Tappa M, Ayuso R, Bodnar RJ, Aylor JG, Jr & Wooden J (2010) Geochronological constraints on the origin of the Coles Hill uranium deposit, Virginia. Geological Society of America, Abstracts with Programs, Vol. 42, No. 1, Abstract #36-9.

Tappa M, Bodnar RJ, Ayuso RA, Aylor JG, Jr, Wooden JL & Vazquez JA (2010) Zircon U/Pb geochronology of host rock and mineralization at the Coles Hill uranium deposit, Virginia. Geological Society of America, Abstracts with Programs, Vol. 42, No. 5, Paper no. 228-9.

Aylor, JG Jr., Beard J, Bodnar RJ & Tappa M (2011) Geology and geochemistry of the Coles Hill uranium deposit. Geological Society of America, Southeastern Section Meeting, March 23-25, 2011, Wilmington, NC, Paper No. 17-3.

Research supported by the U.S. Geological Survey (USGS), Department of the Interior, under USGS award number G09AP00041. The views and conclusions contained in this document are those of the authors and should not be interpreted as necessarily representing the official policies, either expressed or implied, of the U.S. Government.

Age and petrogenesis of host rocks at the Coles Hill uranium deposit, Pittsylvania County, Virginia, USA, based on zircon U-Pb geochronology

Tappa, M.J.[1,2,7], Ayuso, R.A.[2], Bodnar, R.J.[1], Aylor, J.G.[3], Beard, J.[4], Henika, W.S.[1], Vazquez, J.A.[5], and Wooden, J.L.[6]

[1.] Department of Geological Sciences, Virginia Polytechnic Institute and State University, Blacksburg, VA 24061

[2.] United States Geological Survey, Reston, VA 20192

[3.] Virginia Uranium Inc., Chatham, VA 24531

[4.] Virginia Museum of Natural History, Martinsville, VA 24112

[5.] United States Geological Survey, Menlo Park, CA 94025

[6.] Department of Geological and Environmental Sciences, Stanford University, Stanford, CA 94305

[7.] Presently at: Jacobs Technology/ESCG, NASA-JSC, Houston, TX 77058

ABSTRACT (250 word limit)

The Coles Hill uranium deposit, located in south-central Virginia, represents the largest undeveloped uranium deposit in the United States, yet a comprehensive genetic model is yet to be developed for the deposit. This is due, in part, to uncertainties concerning the identification and classification of the hydrothermally-altered meta-igneous rocks that host uranium mineralization. Previously it was assumed that the host rocks represent part of the regional Martinsville Intrusive Complex, although that assessment is largely based on the geographical proximity rather than well-established field observations or geochemical data. Determining of

the host rocks has important implications concerning the development of a uranium exploration program for the region.

Here we present new zircon SHRIMP U-Pb geochronology data, as well as zircon trace element data, for both the mineralized host rocks at Coles Hill and surrounding rocks from the Martinsville Intrusive Complex. Our data confirm that the host rocks at Coles Hill are cogenetic with the broad range of ages for the Martinsville Intrusive Suite that have been determined here and elsewhere. Additionally, our results indicate that a biotite gneiss unit that was previously thought to be part of the Precambrian Fork Mountain Formation is instead a member of the Martinsville Intrusive Complex.

INTRODUCTION

The Coles Hill uranium deposit is located in the western-Piedmont of Pittsylvania County, Virginia (Fig. 1, inset, upper left), approximately 10 kilometers northeast of Chatham, Virginia. Coles Hill is the largest known and undeveloped uranium deposit in the United States, with a mineral resource estimate of 54 thousand metric tonnes U_3O_8 (cutoff grade = 0.025 wt.% U3O8; Maxwell et al., 2009). The deposit was discovered in the 1970's, and in 1979 Marline Uranium Corporation optioned the property and delineated the extent of mineralization during an extensive drilling program from 1979-1984. A moratorium on uranium mining was enacted by the Virginia legislature in 1982 to allow various state agencies to study the issue and, owing to declining market conditions Marline abandoned the project in 1984. Beginning in 2006, following an increase in uranium prices, a newly formed entity, Virginia Uranium, Inc., acquired the property and initiated new studies to better characterize the nature and extent of mineralization in anticipation of future mining of the deposit.

Mineralization at Coles Hill is epigenetic and occurs in fractures in highly brecciated and mylonitized meta-igneous rocks. Most of the uranium at Coles Hill is hosted by the uranium silicate mineral coffinite [$U(SiO4)_{1-x}(OH)_{4x}$] and by uranium oxides (uraninite or pitchblende). One unusual aspect of the deposit is that U-bearing apatite is abundant and may constitute 4% or more of the reserves. A comprehensive genetic model is yet to be developed for the Coles Hill deposit, in part due to uncertainties concerning the age of mineralization and the age and classification of the host rocks in terms of local and regional geology.

The host rocks at Coles Hill have been assumed to be part of the regional Martinsville Intrusive Complex (MIC; Conley, 1985). The MIC consists of the Leatherwood Granite and the Rich Acres Formation (termed “amphibolite” in most early reports) that is intrusive into the Leatherwood Granite (Aylor et al., 2009). The petrologically heterogeneous Leatherwood Granite exhibits a discontinuous outcrop pattern and is one of the prominent igneous units in terms of mapped area within the western-Piedmont of Virginia. Although it is referred to as “granite”, the Leatherwood includes a wide variety of rock types ranging from granodiorite to granite, some of which have undergone deformation and metamorphism to orthogneiss, including rocks exposed in the area immediately surrounding Coles Hill (Conley, 1985). Mafic (amphibolite) units within the Leatherwood Granite are considered to be late intrusions of Rich Acres Formation and field relationships demonstrate that the amphibolite intrudes into the orthogneiss (Henika, 2002). Parts of the Rich Acres Formation exhibit a ductile fabric and these are sometimes referred to as “augen” mylonites. In the vicinity of Coles Hill, the ductile deformation is overprinted by brittle hydrothermal fractures that host the ore. Thus, based on field and petrographic evidence, the ore post-dates the host rock and the period of ductile

deformation, but the amount of time separating the host rock brittle fracturing event from the ore emplacement event is unclear and may be contemporaneous.

The complex lithology and textures of the MIC result from both brittle and ductile deformation and from hydrothermal alteration of the host rocks at Coles Hill. The MIC is widely distributed in this region and, if the host rocks are indeed part of the MIC, this would represent an important factor in developing both a genetic model for the Coles Hill deposit and in identifying future uranium exploration targets in the region, especially if it can be determined that the source of the uranium is the meta-igneous host rock. Additionally, even if these units are not the direct source of the uranium, the igneous rocks could provide a favorable environment for uranium deposition, owing to the abundance of reduced iron-bearing phases such biotite, amphibole and pyroxene that could promote precipitation of uranium as a result of fluid-mineral reactions (c.f. Raffensperger and Garven, 1995).

Here we present new U-Pb zircon geochronology that establishes the age of the mineralized and unmineralized MIC rocks (Leatherwood Granite and Rich Acres Formation) in the vicinity of the Coles Hill deposit. The new age data confirm earlier interpretations that the host rocks at Coles Hill and the MIC are of similar age (Wilson, 2001) and provide the first ages for the mineralized rocks at Coles Hill. We note, however, that all of the units analyzed in this study have undergone metamorphism, and zircon growth could have occurred during metamorphism or igneous emaplacement, or both. In an effort to assess whether the zircons are of igneous or metamorphic origin we have also examined the trace-element chemistry of the zircons.

GEOLOGIC BACKGROUND

The Coles Hill deposit is situated west of the 60°SE dipping Chatham Fault (Fig. 1) within a complex cataclastic and mylonitic zone up to 500 meters wide in the vicinity of the deposit (Henika, 2002). The Chatham Fault separates sedimentary rocks of the Triassic Dan River Basin (also referred to as the Danville Basin in Virginia) to the east from crystalline rocks of the Smith River Allochthon (SRA) to the west (Fig. 1). The SRA is a Paleozoic thrust sheet consisting of late Proterozoic pelitic schists, granitic and pelitic gneisses, and amphibolites of the Basset and Fork Mountain Formations, which are intruded by the MIC (Conley and Henika, 1973). The MIC consists of granite and granodiorite with minor syenite and quartz diorite (Leatherwood Granite) and a slightly younger mafic intrusive unit (Rich Acres Formation) consisting of olivine gabbro, gabbro, diorite and norite some of which are found as dikes that cut through the Leatherwood Granite (Conley, 1985; Conley and Henika, 1973). The Coles Hill deposit occurs exclusively in deformed SRA rocks immediately to the west of the Chatham Fault zone bounding the zone of cataclasis, and structurally above an easterly dipping biotite gneiss unit that is truncated by the Chatham Fault. Owing to similar lithologies, the biotite gneiss unit was previously thought to be part of the Precambrian Fork Mountain Formation (Carter et al., 2006; Conley, 1985). Our geochronology data (see below) suggest that instead it is an additional member of the MIC.

Mineralization at Coles Hill occurs as two main ore bodies, both of which are exclusively hosted in SRA crystalline rocks. The locations of ore bodies shown on Figure 1 are surface projections, and because the ore bodies dip to the southeast, they appear to occur on both sides of the Chatham Fault in Figure 1. However, in the subsurface, uranium mineralization does not extend beyond the zone of intense cataclasis and brecciation and into the Triassic sedimentary rocks of the Triassic Dan River Basin that are located east of the Chatham Fault.

SAMPLE DESCRIPTION

Seven samples were collected for zircon U-Pb SHRIMP and LA-ICPMS trace-element analysis. Five of the samples were collected from surface exposures (RA09-CH1, RA09-CH2, SPG-223) and drill core (S6-03-1 and S6-03-2) in the vicinity of Coles Hill but outside of the mineralized zone (Fig. 1). Two samples (41-90A-1 and 41-90A-2) were collected from drill core within the zone of uranium mineralization (Fig. 1). For each sample, zircon was isolated using standard density (Wilfley or Rodgers Table, methylene iodide) and magnetic (Frantz isodynamic separator) separation techniques. Samples were processed at the U.S. Geological Survey, Reston, VA and the University of North Carolina at Chapel Hill, NC.

Unmineralized Leatherwood Granite orthogneiss

Three samples of the Leatherwood Granite orthogneiss (RA09-CH1, RA09-CH2, SPG-223) were collected from outcrops in the vicinity of, but outside of, the mineralized zone of the Coles Hill deposit (Fig. 1). Zircons from the unmineralized Leatherwood Granite orthogneiss samples are primarily pale to honey-colored euhedral prisms. Samples RA09-CH1 and RA09-CH2 yielded a higher abundance of zircons and more diverse crystal morphologies compared to sample SPG-223. The majority of zircons display moderate length to width aspect ratios (2-3:1), although zircons from samples RA09-CH1 and RA09-CH2 display both high (>4:1) and low (<2:1) aspect ratio populations. Cathodoluminescence (CL) imaging reveals most grains are moderately luminescent and have oscillatory core to rim zones (Fig. 2) typical of magmatic zircon (Kempe et al., 2000; Pidgeon, 1992). Few zircons enclose an obvious xenocrystic core characterized by unconformable and truncated zones within the crystal rim (e.g. Fig. 2, RA09-CH1 second from left).

Unmineralized Rich Acres Formation amphibolite

One sample of the Rich Acres Formation amphibolite (S6-03-1) was collected from a depth of 184 to 194 ft. from a drill hole that was collared in the MIC approximately 200 m southwest of the South ore body (Fig. 1, inset location labeled “03”) and which did not intersect economic mineralization (although the rocks are hydrothermally altered). Zircons are primarily clear to honey-colored euhedral to subhedral prisms that are commonly fractured and contain inclusions of oxide minerals. CL imaging shows that most grains display multiple zones with varying degrees of luminescence. Nearly all grains display large wavy CL zones, rather than the thin oscillatory zones observed in zircons from the other six samples (Fig. 2).

Mineralized Leatherwood Granite orthogneiss

One sample from the mineralized gneissic host rock (41-90A-1) was collected from a depth of 497.8 to 507.2 ft. from a drill hole within the North ore body at Coles Hill (Fig. 1, inset location labeled “90A”). The sample contained abundant fractures containing uranium-bearing minerals, which were processed along with the host rock gneiss during zircon separation. The core was assayed over two-foot intervals, and average uranium grades for the six two-foot intervals that included the depth range sampled varied from 0.034 to 0.731 wt.% U_3O_8. Zircons separated from the mineralized host rock orthogneiss are primarily pale to honey-colored and euhedral. CL imaging demonstrates that nearly all grains display core to rim oscillatory zoning, with core structures that vary from low to high luminescence (Fig. 2).

Mineralized Rich Acres Formation amphibolite

One sample of mineralized amphibolitic host rock (41-90A-2) was collected from drill core. The sample was from the same drill hole as sample 41-90A-1, but from a depth of 635.2 to 644.5 ft. below the surface (Fig. 1, inset location labeled “90A”). As described above for sample

41-90A-1, this sample also contained numerous mineralized fractures that were processed along with the amphibolite during zircon separation. The core was assayed over two-foot intervals, and average uranium grades for the six two-foot intervals that included the depth range sampled varied from 0.069 to 0.705 wt.% U_3O_8. Zircons isolated from the mineralized amphibolite are typically pale-yellow, euhedral to subhedral, and are often fractured. CL imaging reveals that most grains display multiple zones with varying degrees of luminescence. Similar to the zircons isolated from the unmineralized Rich Acres Formation amphibolite sample, many grains display large wavy CL zones, rather than the thin oscillatory zones.

MIC biotite gneiss

One sample of the unmineralized MIC biotite gneiss (S6-03-2) that forms the footwall to the zone of mineralization was collected from the same drill hole as sample S6-03-1, but from a depth of 1336 to 1343 ft. (Fig. 1, inset location labeled “03”). This section of drill core was not mineralized and the uranium grade is not available. Zircons isolated from the biotite gneiss are typically clear to pale-yellow euhedral prisms. CL imaging demonstrates that nearly all zircons display core to rim oscillatory zoning with varying degrees of luminescence. Zircons often display a low luminescent core showing a variety of different textures, and the core is surrounded by a higher luminescent rim. This unit was previously thought to be part of the Fork Mountain Formation based on its stratigraphic location beneath other rocks interpreted to be part of the MIC, and based on its similar appearance to outcrops of Fork Mountain Schist in the region.

ANALYTICAL METHODS

Sample Preparation

For each sample, zircon was inspected under reflected and transmitted light using a binocular microscope. Only grains that were identified to be free, or nearly free, of inclusions

were selected for analysis. Selected grains were mounted in ardalite epoxy, and ground and polished to expose the entire crystal, from core to rim. A carbon coating was applied to the mount and each zircon was photographed in CL to reveal internal zoning (Fig. 2). The carbon coating was removed, and a gold coating was applied prior to SHRIMP analysis.

U-Pb SHRIMP Analyses

Zircon U-Pb analysis was conducted using the Stanford-USGS SHRIMP-RG ion microprobe at Stanford University, CA, during two analytical sessions, one in November 2009 (RA09-CH1, RA09-CH2, SPG-223) and a second in October 2010 (S6-03-1, S6-03-2, 4190A-1, 4190A-2), and closely follows the procedure of Williams (1997). Samples were mounted in epoxy, sectioned to expose zircon interiors, polished, and coated with gold prior to analysis. A primary oxygen beam of mass filtered $^{16}O_2^-$ with intensity of 4-6 nA was focused to an approximately 15-20 micrometer spot using Kohler illumination. To remove surface contaminants, the target area for each zircon was rastered for 2 minutes prior to analysis. Each analysis consisted of five scans through the mass range from $^{89}Y^+$ to $^{238}U^{16}O_2^+$. Uranium concentrations are referenced to the MAD zircon (4196 ppm U, Yui et al., 2010) and zircon standard R33 (419 Ma, Black et al., 2004) was used to normalize measured U-Pb ratios for age calculations. Standard R33 was analyzed after every three to five unknown analyses throughout the duration of each analytical session. Raw data were reduced, mean ages calculated, and data were graphically portrayed using the SQUID (v. 1.03; Ludwig, 2001) and Isoplot (v. 3.0; Ludwig, 2003) software programs.

Trace Element Analyses

Zircon trace element analysis was conducted simultaneously with U-Pb analysis for samples S6-03-1, S6-03-2, 4190A-1 and 4190A-2 on the SHRIMP-RG system at Stanford

University. For samples RA09-CH1, RA09-CH2, and SPG-223, trace-element analysis was conducted following SHRIMP analysis using an Agilent 7500ce LA-ICPMS system at Virginia Tech during two analytical sessions in January and February 2010. For these latter samples, trace-element analysis was conducted following U-Pb analysis, and after the gold coating was removed. For each LA-ICPMS analysis, the laser was focused into the center of the pit created during SHRIMP analysis in an attempt to assure both analyses were conducted within the same crystal zone. However, we cannot be certain that multiple zones were not intersected and sampled at different depths during the ablation process.

LA-ICPMS analyses were conducted using a GeoLas Pro ArF excimer laser with output energy of 150 mJ and energy density on the sample of approximately 7-10 J/cm^2, and repetition rate of 5 Hz. The ablation cell volume is approximately 1.5 cm^3, and He carrier gas flow was ≈0.9 L/min. During analysis, the dwell time per isotope was 10 ms, and NIST 610 glass was used as the standard. The standard was analyzed twice at the beginning and at the end of each analytical session. Previous workers have shown that abundances of most elements in silicate phases, including the rare earth elements and many of the alkaline earth and high field strength elements, can be determined with better than 10% accuracy using the NIST 610/612 standards combined with a 193 nm excimer laser (Guillong et al., 2003; Sylvester, 2008). Data were reduced using the AMS software package (Mutchler et al., 2008).

RESULTS

The goal of this study was to identify and determine the ages of host rocks at the Coles Hill uranium deposit within the context of known regional geological relationships. This information is required to constrain the geological sources, controls, and timing of uranium mineralization at Coles Hill. To achieve this goal, zircon U-Pb SHRIMP analyses were

performed on three unmineralized Leatherwood Granite samples, one unmineralized Rich Acres Formation amphibolite sample, and one unmineralized MIC biotite gneiss sample collected near Coles Hill but outside of the known area of mineralization. Two samples of the mineralized host rock containing economic uranium grades were also analyzed. For each analysis, the ion beam was placed such that it was contained within an area of the crystal that showed a homogeneous CL pattern, and an effort was made to acquire a substantive dataset of both cores and rims for each sample. Examples of spot locations for several crystals are shown in Figure 2.

Zircons from all samples yield concordant analyses that span the same general age range and display large age variability within individual samples (supplemental material; Concordia plots). Samples of the Leatherwood Granite orthogneiss display the largest variability (>100 My). This variability is not easily explained, as it does not directly correlate with the location of analysis (core vs. rim) or with any measured chemical parameter including U concentration or abundance of common Pb (supplemental material, Table 1). Additionally, the age variability cannot be attributed to analytical error, because the standard does not yield the same variability and the data were collected during two analytical sessions (supplemental material, Table 2). The variability complicates the assignment of sample mean ages because the ages obtained from different zircons from each individual sample largely do not overlap. In order to eliminate any potential bias when selecting the cluster of analyses (ages) used to calculate the best age estimate, we follow the method of Castenias et al. (2010) and use the algorithm TuffZirc (Ludwig and Mundil, 2002), which is designed to identify and calculate the mean of the most coherent and reliable group of ages in a dataset containing some analysis affected by positive and negative age biases. If the data that are input into the TuffZirc algorithm are concordant, precise, cogenetic, and with the majority unaffected by Pb-loss, the algorithm output should represent

crystallization ages. In order to satisfy these conditions, data points that were discordant, imprecise, or showed signs of inheritance (based on age and CL imaging) were removed from the dataset prior to incorporation into the algorithm. Additionally, spurious data points significantly younger than the majority of other ages are likely the result of disruption of the U/Pb systematics (e.g. Pb-loss) and are not included in algorithm input. Analytical results for all zircon analyses, including those not included in the TuffZirc algorithm, are listed in Table 1 and shown on Figure 3.

Leatherwood Granite orthogneiss

Three samples of the Leatherwood Granite orthogneiss all yield similar $^{206}Pb/^{238}U$ zircon ages that span the same overall range (approximately 400-522 Ma). The mean age does not vary as a function of spot location (rim vs. core), crystal morphology (l/w ratios), or degree of CL luminescence for any of the samples.

Fifty-two analyses of 33 zircons from sample RA09-CH1 yield $^{206}Pb/^{238}U$ ages that range from 402 to 522 Ma, with the exception of three zircon core analyses that yield ages between 1028 and 1152 Ma and which appear to represent inherited xenocrysts (Fig. 2). Those three analyses (CH1R1-9.1, R2-5.1, R1-7.1) along with another analysis (R1-7.1) were not included in the TuffZirc algorithm due to potential inheritance. Also removed from the algorithm input were nineteen discordant and/or imprecise analyses (R1-16.1, R1-3.2, R1-5.2, R1-14.1, R2-1.1, R1-5.1, R1-14.3, R1-10.1, R2-4.1, R1-12.1, R1-15.1, R1-1.2, R2-9.1, R1-21.1, R2-1.2, R1-6.3, R1-24.1, R1-22.1, and R1-6.2; Table 1). TuffZirc identified a coherent cluster of fourteen analyses near the median of the distribution that yield a mean age of 439.4 (+3.7, -2.4) Ma (1σ).

Fifty-seven analyses of 33 zircons from sample RA09-CH2 yield $^{206}Pb/^{238}U$ ages that range from 403 to 503 Ma. One other analysis, of a zircon core, yields an age of 1192 Ma on a

single spot. Several analyses were not considered for the TuffZirc algorithm for a series of reasons which include inheritance (CH2R1-11.1, R2-2.1), discordance and/or imprecision (R1-5.1, R2-7.1, R1-4.1, R2-8.1, R1-4.2, R1-1.1, R1-3.2, R1-14.1, R2-5.1, R2-6.2, R2-9.2, R1-9.2, R1-10.3, R2-6.1, R2-1.1, R1-9.1, R2-8.2, and R2-5.2; Table 1). TuffZirc identified a coherent cluster of nineteen analyses slightly older than the median that yield a mean age of 455.6 (+1.0, -1.6) Ma (1σ).

Forty-three analyses of 34 zircons from sample SPG-223 yield ^{206}Pb /^{238}U ages that range from 200 to 480 Ma. One other analysis, of a zircon core, yields an age of 1044 Ma. That analysis (33.1), along with another analysis (6.1) was not considered for the TuffZirc algorithm due to potential inheritance. Analyses 17.1, 14.1, 16.1, and 19.1 are not included in the TuffZirc input due to potential Pb-loss, and analyses 15.1 and 21.1 were removed due to discordance (Table 1). TuffZirc identifies a coherent cluster of eleven analyses near the median that yield a mean age of 432.5 (+2.3, -1.6) Ma (1σ).

Rich Acres Formation amphibolite

Sixteen analyses of 16 zircons from sample S6-03-1 yield ^{206}Pb /^{238}U ages that range from 406 to 438 Ma. Only one spot analysis was obtained for each zircon from this sample. All data are concordant and were input into the TuffZirc algorithm (Table 1). TuffZirc identified a coherent cluster of the thirteen oldest analyses that yields a mean age of 425.2 (+9.4, -7.7) Ma (1σ).

Mineralized Leatherwood Granite orthogneiss

Nineteen analyses of 17 zircons from sample 41-90A-1 yield ^{206}Pb /^{238}U ages that range from 381 to 450 Ma. Three data points were removed from algorithm input due to discordance

(16.1, 3.1) and potential Pb-loss (1.1) (Table 1). TuffZirc identified a coherent cluster of nine analyses slightly younger than the median that yield a mean age of 426.1 (+6.8, -5.7) Ma (1σ).

Mineralized Rich Acres Formation amphibolite

Twenty-three analyses of 16 zircons from sample 4190A-2 yield $^{206}Pb/^{238}U$ ages that range from 343 to 506 Ma. The distribution of ages for this sample shows a noticeable "step" at approximately 430 Ma, which separates 12 analyses yielding older ages from 11 analyses yielding younger ages (Table 1). Using the total analysis range, TuffZirc identifies a coherent cluster of nine analyses from the older group that yield a mean age of 440.3 (+9.1, -4.4) Ma (1σ). If the dataset is limited to only those analyses that are younger than the age at which the step occurs, TuffZirc identified a coherent cluster of six analyses and yields a mean age of 415.7 (+6.2, -9.6) Ma. As stated above, field relationships document that the mineralized orthogneiss must be older than the mineralized amphibolite, therefore the younger mean age is the preferred age of crystallization and the older age may reflect inheritance. Six analyses were not considered in the TuffZirc algorithm due to discordance (2.1, 2.2, 4.2, 3.1, 12.1), and imprecision (14.1; Table 1).

MIC biotite gneiss

Twenty-two analyses of 21 zircons from sample S6-03-2 yield $^{206}Pb/^{238}U$ ages that range from 356 to 598 Ma. Two analyses were not considered in the algorithm input due to discordance (S6-03-2 16.1) and possible Pb-loss (20.1; Table 1). TuffZirc identified a coherent cluster of the ten oldest analyses that yields a mean age of 431.3 (+4.2, -12.5) Ma (1σ).

Trace-element composition

Rare earth element and hafnium (Hf) abundances were measured in all zircons investigated for geochronology. For samples S6-03-1, S603-2, 4190A-1, 4190A-2, La, Ce, Pr,

Nd, Sm, Eu, Gd, Dy, Y, Er, Yb were measured on the SHRIMP as part of the U-Pb analytical protocol. For samples RA09-CH1, RA09-CH2, and SPG-223, La, Ce, Sm, Eu, Dy, and Y were measured by LA-ICPMS on the same grains following SHRIMP analysis. Results for the four samples analyzed on the SHRIMP are listed in Table 3 (supplemental material), and those from the LA-ICPMS are listed in Table 4 (supplemental material). In general, zircons from all samples appear to have similar trace element patterns although their absolute abundances may vary. Normalized to chondritic values, La and Pr concentrations in zircon are on average depleted, HREE concentrations are enriched, and positive Ce and negative Eu anomalies are observed in all samples. REE diagrams showing trace element abundances for the samples analyzed by the SHRIMP are shown on Figure 4. Owing to the small number of elements analyzed by LA-ICPMS the data are not plotted on Figure 4, but show similar trends (Table 4).

DISCUSSION

Zircon Petrogenesis

The Piedmont region of the central Appalachians has experienced a long and complicated geologic history. That history includes multiple regional metamorphic events (the Taconic, Acadian, and Alleghanian Orogenies) that occurred during or after intrusion of the MIC and the rocks that host uranium mineralization at Coles Hill (Carter et al., 2006; Gates, 1997; Hibbard et al., 2003). Understanding if and/or how these post-MIC metamorphic events contribute to the ages yielded by the zircons is critical to understanding the genetic relationship between the units investigated.

No single diagnostic chemical or physical feature can unequivocally distinguish between zircon of igneous and metamorphic origin (Hoskin and Schaltegger, 2003). However, multiple lines of evidence suggest that the zircons analyzed in this study are of igneous origin. These

include: (1) the subhedral and prismatic crystal morphology typical of igneous zircons (Hoskin and Schaltegger, 2003); (2) the core to rim internal zoning and lack of grains that display low CL luminescent cores and bright luminescent rims, as is found in some metamorphic zircons (Schaltegger et al., 1999); (3) the lack of a systematic age difference between crystal cores and rims, which signifies that late stage overgrowths are generally not observed and crystallization likely occurred via a single process; (4) the depletion of LREE, enrichment of HREE, and positive Ce and negative Eu anomalies that are typical of zircons that crystallized from a silicate melt (Fig. 4; Hoskin and Schaltegger, 2003); (5) the absence of very low Th/U ratios (<0.07) commonly found in metamorphic zircons (Rubatto, 2002); and (6) the rarity of zircons that contain high Th concentrations and sufficiently high U/Ce ratios and plot within the metamorphic field on the igneous/metamorphic discrimination plot (Fig. 5; Castiñeiras et al., 2010). None of these observations proves conclusively that the zircons are of igneous origin, but all are consistent with the interpretation that the zircons analyzed in this study crystallized from a silicate melt.

While it appears that the zircons are not of metamorphic origin, a thermal event resulting in Pb-loss may be responsible for some of the age variability observed within the samples (Cherniak and Watson, 2001). Lead loss could be related to the massive thermal event that accompanied intrusion of the Atlantic Magmatic Province diabase and basalt dikes and sills along the Eastern Seaboard. Independent geochemical studies (Henika, 2011) show that the Triassic metasediments in the Coles Hill area were metamorphosed to zeolite and to chlorite grade at some time after the intrusion of the Jurassic basaltic intrusions that were also altered by the event. Given the significant age variability observed in all samples and the complicated thermal history that these rocks have undergone, it is likely that at least some of the zircons have

experienced Pb-loss. Identifying the extent of Pb-loss from individual zircon crystals is a complex process and not within the realm of this study. We acknowledge that it is possible that the results we report here may be skewed to younger ages owing to Pb-loss and that the actual crystallization age may be older than the mean age reported here. However, independent geochronology data suggests otherwise.

Tracy et al. (2001) determined the timing of the Rich Acres intrusion by dating metamorphic monazite from the Fork Mountain schist that is within the contact aureole of a Rich Acres norite intrusion. They report a U-Th-Pb monazite age of 433±12 Ma. Unlike zircon, monazite does not become metamict with radiation damage and therefore is less susceptible to Pb-loss (Cherniak et al., 2004). The monazite age Tracy et al. (2001) report is in agreement with the age reported here for the unmineralized Rich Acres Formation (425.2 +9.4, -7.7 Ma), thus supporting the interpretation that the mean ages presented here are recording the crystallization age and not a later Pb-loss event.

Age of the MIC in the vicinity of Coles Hill

The U-Pb zircon data presented here (Table 1) establishes the crystallization ages for the Leatherwood Granite and Rich Acres Formation in the vicinity of Coles Hill. Zircons from three samples of the Leatherwood orthogneiss yield statistically distinguishable mean ages between 431-457 Ma (Fig. 3). These ages are broadly consistent with previous geochronological studies on the Leatherwood Granite that includes a zircon U-Pb TIMS age of 450 Ma (Rankin, 1975), and zircon U-Pb SIMS mean ages of 444±9 and 441±8 Ma (Wilson, 2001), with the latter age obtained from an orthogneiss sample collected near Coles Hill. The combined data suggest a protracted crystallization history for the Leatherwood Granite. Zircons from the Rich Acres Formation amphibolite yield similar results but with a slightly younger mean age (425.2 +9.4, -

7.7 Ma) that is consistent with the age of 430±7 Ma reported by Wilson (2001). These results support the interpretation that the inter-layered amphibolite was intruded as late-stage mafic dikes prior to metamorphism (Aylor et al., 2011).

As stated above, prior to this investigation the biotite gneiss unit that underlies mineralization at Coles Hill was thought to be part of the Fork Mountain Formation. The age of the biotite gneiss reported here (431.3 +4.2 -12.5 Ma) is significantly younger than the ages reported for nearly all units of the Precambrian Fork Mountain Formation (Carter et al., 2006; Hibbard et al., 2003), with one notable exception. In a detrital zircon study of the SRA, Carter et al. (2006) report a large population of zircon yielding U-Pb ages between 420 and 460 Ma for a migmatitic biotite gneiss unit. While a detailed description of that unit is not provided by Carter et al. (2006), it is probable that it is the equivalent of the MIC biotite gneiss described here based on the proximity to MIC rocks (Fig. 4 in Carter et al., 2006) and the age of the zircon. Carter et al. (2006) interpreted these ages to reflect metamorphic zircon growth, and not the crystallization age of the unit, yet we have documented that all of the zircons studied here, including those from the biotite gneiss, were likely derived from an igneous melt. We therefore suggest that the younger population of zircons described by Carter et al. (2006) were also derived from an igneous melt, and that the biotite gneiss unit is part of the MIC and not the Fork Mountain Formation.

Are the host rocks at Coles Hill part of the Martinsville Igneous Complex?

The zircon U-Pb data presented here establish that the meta-igneous host rocks for the Coles Hill uranium deposit are within the broad range of ages determined in this study and elsewhere (Rankin, 1975; Wilson, 2001) for the MIC. The mean age for the mineralized

orthogneiss (4190A-1, 426.1 +6.8-5.7 Ma) and the unmineralized Leatherwood orthogneiss sampled closest to the deposit (SPG-223, 432.5 +2.3-1.6 Ma) overlap. The younger mean age for the mineralized amphibolite (4190A-2, 415.7 +6.2-9.6 Ma) and the unmineralized Rich Acres amphibolite (S6-03-1, 425.2 +9.4-7.7 Ma) overlap. Based on these temporal relationships, we conclude that the host rocks at Coles Hill are coeval with the Leatherwood Granite and Rich Acres Formation, both of which are included as members of the MIC.

Implications for future uranium exploration in the region

Two models are currently being considered concerning the source of the uranium in the Coles Hill deposit. One model assumes that the uranium is sourced locally from the meta-igneous host rocks or from an unexposed intrusion at depth. A second model considers the Triassic sedimentary rocks of the Danville Basin to be the source of the uranium (Aylor and Bodnar, 2010). Geochronological results from this study do not preclude either of these inferred sources. If the source of the uranium is the meta-igneous host rocks, mineralization could have formed shortly after the rocks cooled sufficiently to undergo brittle deformation. Conversely, if the Triassic sediments in the Danville Basin are the source of uranium at Coles Hill, mineralization would have occurred at least 200 Ma after intrusion of the MIC. The data presented here do not preclude either of the proposed sources, but do provide a firm basis for future geological, geochemical and structural studies designed to constrain the uranium source(s) for the Coles Hill mineralization, and to determine the age of the mineralization.

SUMMARY

1. Zircons from the mineralized orthogneiss and mineralized amphibolite host rocks at the Coles Hill uranium deposit yield mean ages that are statistically similar to zircons from the Leatherwood Granite orthogneiss and Rich Acres Formation amphibolite, respectively. This supports earlier suggestions that the host rocks are deformed members of these units, which are part of the Martinsville Igneous Complex. Additionally, data indicate a protracted crystallization history (10's M.y.) for the Leatherwood Granite and later intrusion of the Rich Acres formation.
2. The biotite gneiss unit that underlies the mineralized zone is not a member of the early Cambrian Fork Mountain Schist as has been previously assumed (Carter et al., 2006). Zircons from the biotite gneiss yield ages similar to ages reported for rocks of the MIC, and the basal biotite gneiss unit is now interpreted to be part of the MIC.
3. The wide range in ages observed in zircons from all samples is not the result of metamorphic overprinting. Zircon Pb-loss could contribute to some of the observed spread in ages, although the mean ages are consistent with the timing of intrusions determined by other methods.

ACKNOWLEDGEMENTS

The authors thank Luca Fedele for his assistance with the LA-ICPMS system at Virginia Tech. We also thank John Jackson and Drew Coleman for their assistance in the processing of samples, and Stewart East for assistance in sample collection. We thank Brad Ito for providing critical electronics support for the SHRIMP-RG ion microprobe. Funding for this project was provided by a grant to RJB and RAA from the U.S. Geological Survey Mineral Resources External Research Program (MRERP). The curation staff at the Virginia Museum of Natural

History generously provided access to drill core 41-90A from which samples (41-90A-1, 41-90A-2) were collected. Reviews of an earlier version of this manuscript by Robert Tucker and Gilpin Robinson significantly improved the presentation.

FIGURE CAPTIONS

Figure 1: Simplified regional geologic map of the mid-Piedmont region in south-central Virginia (modified from Henika, 2002) with insets showing the location of Coles Hill in southside Virginia (upper left) and the local geology (lower right) in the vicinity of the Coles Hill uranium deposit. The surface projections of the north and south ore bodies at Coles Hill are shown on the lower inset. The black stars represent sample location and sample names are abbreviated for clarity. (CH1 = RA09-CH1; CH2 = RA09-CH2; 223 = SPG-223; 03 = S6-03-1 and S6-03-2; 90A = 4190A-1 and 4190A-2)

Figure 2: Cathodoluminescence images for selected zircons from each sample. The dashed circle represents the approximate location of a SHRIMP analysis and the number corresponds to the $^{206}Pb/^{238}U$ age (in Ma) determined for that analysis.

Figure 3: Selected results of zircon U-Pb SHRIMP geochronology. All plots constructed using the ISOPLOT software program (Ludwig, 2003) and mean ages calculated using the algorithm TuffZirc (Ludwig and Mundil, 2002). Error bars in $^{206}Pb/^{238}U$ mean age plots are plotted at $\pm 2\sigma$, and $^{206}Pb/^{238}U$ ages are corrected by ^{207}Pb. Analyses with red error bars are included in the mean age calculation (represented as green bands), whereas analyses with blue error bars were deemed outliers by the algorithm. Empty error bars represent analyses not included as input into the algorithm due to inheritance, discordance, imprecision, or potential Pb-loss. Due to the noticeable step or discontinuity in ages in sample 41-90A-2, two mean ages were calculated and

the younger mean age is represented as a yellow band. Summary of mean ages from all samples is plotted in lower right.

Figure 4: Chondrite-normalized rare earth element (REE) and Y plot for the samples analyzed using the SHRIMP-RG system. Individual lines represent a single analysis. Normalized to the chondrite values provided by Anders and Grevesse (1989) and modified by Korotev (1996).

Figure 5: Concentration of thorium versus U/Ce in the zircons analyzed. The 1:1 line distinguishes metamorphic zircon (upper left) from igneous zircon (lower right) as described by Castiñeiras et al. (2010).

Supplemental material:

Concordia plots: Conventional "Wetherill" concordia plots for all samples of U/Pb zircon data regressed using the TuffZirc algorithm. For clarity, only the data used by TuffZirc in the mean age calculations were plotted for samples RA09-CH1, RA09-CH2, and SPG-223 due to the more extensive number of analyses preformed on these samples the wide range of ages input into the algorithm. All data input into the algorithm is plotted for samples 4190A-1, 4190A-2, S6-03-1, and S6-03-2. Error ellipses are plotted at 2σ.

REFERENCES

Anders, E., and Grevesse, N., 1989, Abundances of the elements; meteoritic and solar: Geochimica Et Cosmochimica Acta, v. 53, p. 197-214.

Aylor, J., Beard, J., and Bondar, R., 2009, Coles Hill, Chatham, Virginia uranium deposit: Abstracts with Programs - Geological Society of America, v. 41, p. 48.

Aylor, J.G.J., Beard, J., Bondar, R.J., and Tappa, M., 2011, Geology and geochemistry of the Coles Hill uranium deposit: Geological Society of America Abstracts with Programs, v. 43, p. 69.

Aylor, J.G.J., and Bodnar, R.J., 2010, Current understanding of the Coles Hill uranium deposit, southside Virginia.: Geological Society of America Abstracts with Programs, v. 42, p. 72-3.

Black, L.P., Kamo, S.L., Allen, C.M., Davis, D.W., Aleinikoff, J.N., Valley, J.W., Mundil, R., Campbell, I.H., Korsch, R.J., Williams, I.S., and Foudoulis, C., 2004, Improved Pb-206/U-238 microprobe geochronology by the monitoring of a trace-element-related matrix effect; SHRIMP, ID-TIMS, ELA-ICP-MS and oxygen isotope documentation for a series of zircon standards: Chemical Geology, v. 205, p. 115-140.

Carter, B.T., Hibbard, J.P., Tubrett, M., and Sylvester, P., 2006, Detrital zircon geochronology of the Smith River Allochthon and Lynchburg Group, southern Appalachians: Implications for Neoproterozoic-Early Cambrian paleogeography: Precambrian Research, v. 147, p. 279-304.

Castiñeiras, P., Garcia, F.D., and Barreiro, J.G., 2010, REE-assisted U-Pb zircon age (SHRIMP) of an anatectic granodiorite: Constraints on the evolution of the A Silva granodiorite, Iberian allochthonous complexes: Lithos, v. 116, p. 153-166.

Cherniak, D.J., and Watson, E.B., 2001, Pb diffusion in zircon: Chemical Geology, v. 172, p. 5-24.

Cherniak, D.J., Watson, E.B., Grove, M., and Harrison, T.M., 2004, Pb diffusion in monazite: A combined RBS/SIMS study: Geochimica Et Cosmochimica Acta, v. 68, p. 829-840.

Conley, J.F., 1985, Geology of southwestern Virginia Piedmont: Virginia Division of Mineral Resources Publication, v. 59, p. 33.

Conley, J.F., and Henika, W.S., 1973, Geology of the Snow Creek, Martinsville East, Price, and Spray quadrangles, Virginia: Mineral Resources Report (Charlottesville), v. 33, p. 71.

Gates, A.E., 1997, Multiple reactivations of accreted terrane boundaries; an example from the Carolina Terrane, Brookneal, Virginia: Special Paper - Geological Society of America, v. 314, p. 49-63.

Guillong, M., Horn, I., and Gunther, D., 2003, A comparison of 266 nm, 213 nm and 193 nm produced from a single solid state Nd : YAG laser for laser ablation ICP-MS: Journal of Analytical Atomic Spectrometry, v. 18, p. 1224-1230.

Henika, W.S., 2002, Geologic map of the Virginia portion of the Danville 30x60 minute quadrangle Virginia Division of Mineral Resouces Publication 166.

Henika, W.S., 2011, Mesozoic ductile to brittle deformation - A new paradigm in the southside Virginia piedmont: Geological Society of America Abstracts with Programs, v. 43, p. 23.

Hibbard, J.P., Tracy, R.J., and Henika, W.S., 2003, Smith River allochthon: A southern Appalachian peri-Gondwanan terrane emplaced directly on Laurentia?: Geology, v. 31, p. 215-218.

Hoskin, P.W.O., and Schaltegger, U., 2003, The Composition of Zircon and Igneous and Metamorphic Petrogenesis: Reviews in Mineralogy and Geochemistry, v. 53, p. 27-62.

Kempe, U., Gruner, T., Nasdala, L., and Wolf, D., 2000, Relevance of cathodoluminescence for the interpretation of U-Pb zircon ages, with an example of an application to a study of zircons from the Saxonian granulite complex, Germany, *in* Pagel, M., Barbin, V., Blanc, P., and Ohnenstetter, D., eds., Cathodoluminescence in geosciences: Berlin, Germany, Springer, p. 415-455.

Korotev, R.L., 1996, A self-consistent compilation of elemental concentration data for 93 geochemical reference samples: Geostandards Newsletter-the Journal of Geostandards and Geoanalysis, v. 20, p. 217-245.

Ludwig, K.R., 2001, SQUID 1.02, a user's manuel: Berkeley Geochronology Center Special Publication 2, p. 17.

Ludwig, K.R., 2003, ISOPLOT/Ex, version 3, A geochronological toolkit for Microsoft Excel: Berkeley Geochronology Center Special Publication 4, p. 71.

Ludwig, K.R., and Mundil, R., 2002, Extracting reliable U-Pb ages and errors from complex populations of zircons from Phanerozoic tuffs: Geochimica Et Cosmochimica Acta, v. 66, p. 463.

Maxwell, R.D., Gibbs, B.L., Pool, T.C., Keim, S.K., and Christopher, P.A., 2009, Technical report on the Coles Hill uranium property Pittsylvania County, Virginia, United States of America.

Mutchler, S.R., Fedele, L., and Bodnar, R.J., 2008, Analysis Management System (AMS) for reduction of laser ablation ICPMS data, *in* Sylvester, P., ed., Laser-Ablation-ICPMS in the Earth Sciences: Current Practices and Outstanding Issues, Volume 40, Mineralogical Association of Canada Short Course Series, p. 318-327.

Pidgeon, R.T., 1992, Recrystallization of Oscillatory Zoned Zircon - Some Geochronological and Petrological Implications: Contributions to Mineralogy and Petrology, v. 110, p. 463-472.

Raffensperger, J.P., and Garven, G., 1995, The formation of unconformity-type uranium ore deposits. 2. Coupled hydrogeochemical modeling.: American Journal of Science, v. 295, p. 639-696.

Rankin, D.W., 1975, Continental-Margin of Eastern North-America in Southern Appalachians - Opening and Closing of Proto-Atlantic Ocean: American Journal of Science, v. A275, p. 298-&.

Rubatto, D., 2002, Zircon trace element geochemistry: partitioning with garnet and the link between U-Pb ages and metamorphism: Chemical Geology, v. 184, p. 123-138.

Schaltegger, U., Fanning, C.M., Gunther, D., Maurin, J.C., Schulmann, K., and Gebauer, D., 1999, Growth, annealing and recrystallization of zircon and preservation of monazite in high-grade metamorphism: conventional and in-situ U-Pb isotope, cathodoluminescence and microchemical evidence: Contributions to Mineralogy and Petrology, v. 134, p. 186-201.

Stacey, J.S., and Kramers, J.D., 1975, Approximation of Terrestrial Lead Isotope Evolution by a 2-Stage Model: Earth and Planetary Science Letters, v. 26, p. 207-221.

Steiger, R.H., and Jager, E., 1977, Subcommission on Geochronology - Convention on Use of Decay Constants in Geochronology and Cosmochronology: Earth and Planetary Science Letters, v. 36, p. 359-362.

Sylvester, P., 2008, Chapter 5. Matrix effects in laser ablation ICPMS., *in* Sylvester, P., ed., Laser-Ablation-ICP-MS in the Earth Sciences: Current Practices and Outstanding Issues, Volume 40, Mineralogical Association of Canada Short Course Series, p. 67-78.

Williams, I.S., 1997, U-Th-Pb geochronology by ion microprobe: not just ages but histories: Soc. Econ. Geol. Rev. Econ. Geol., v. 7, p. 1-35.

Wilson, J.R., 2001, U/Pb zircon ages of plutons from the central appalachians and gis-based assessment of plutons with comments on their regional tectonic significance: Blacksburg, VA, Virginia Polytechnic Institute and State University.

Yui, T.F., Maki, K., Usuki, T., Lan, C.Y., Martens, U., Wu, C.M., Wu, T.W., and Liou, J.G., 2010, Genesis of Guatemala jadeitite and related fluid characteristics: Insight from zircon: Chemical Geology, v. 270, p. 45-55.

Figure 1

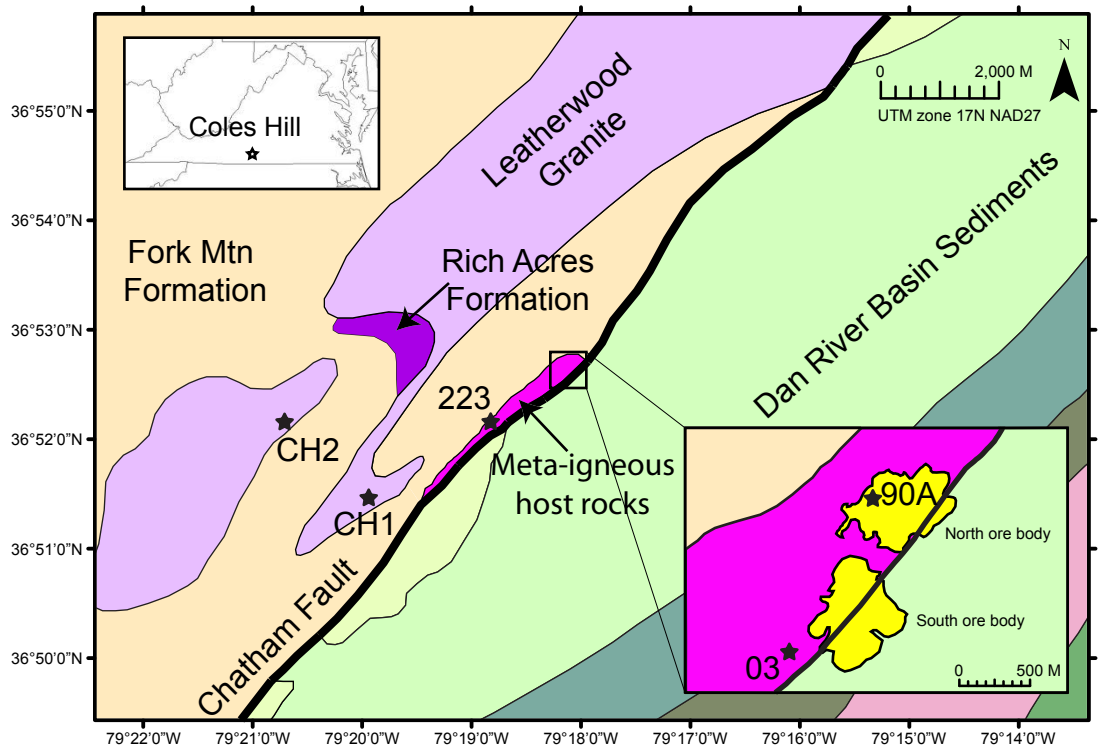
Coles Hill
Leatherwood Granite
Fork Mtn Formation
Rich Acres Formation
Dan River Basin Sediments
223
CH2
CH1
Meta-igneous host rocks
Chatham Fault
0
2,000 M
UTM zone 17N NAD27
N
90A
North ore body
South ore body
03
0
500 M
36°55'0"N
36°54'0"N
36°53'0"N
36°52'0"N
36°51'0"N
36°50'0"N
79°22'0"W
79°21'0"W
79°20'0"W
79°19'0"W
79°18'0"W
79°17'0"W
79°16'0"W
79°15'0"W
79°14'0"W

Figure 2

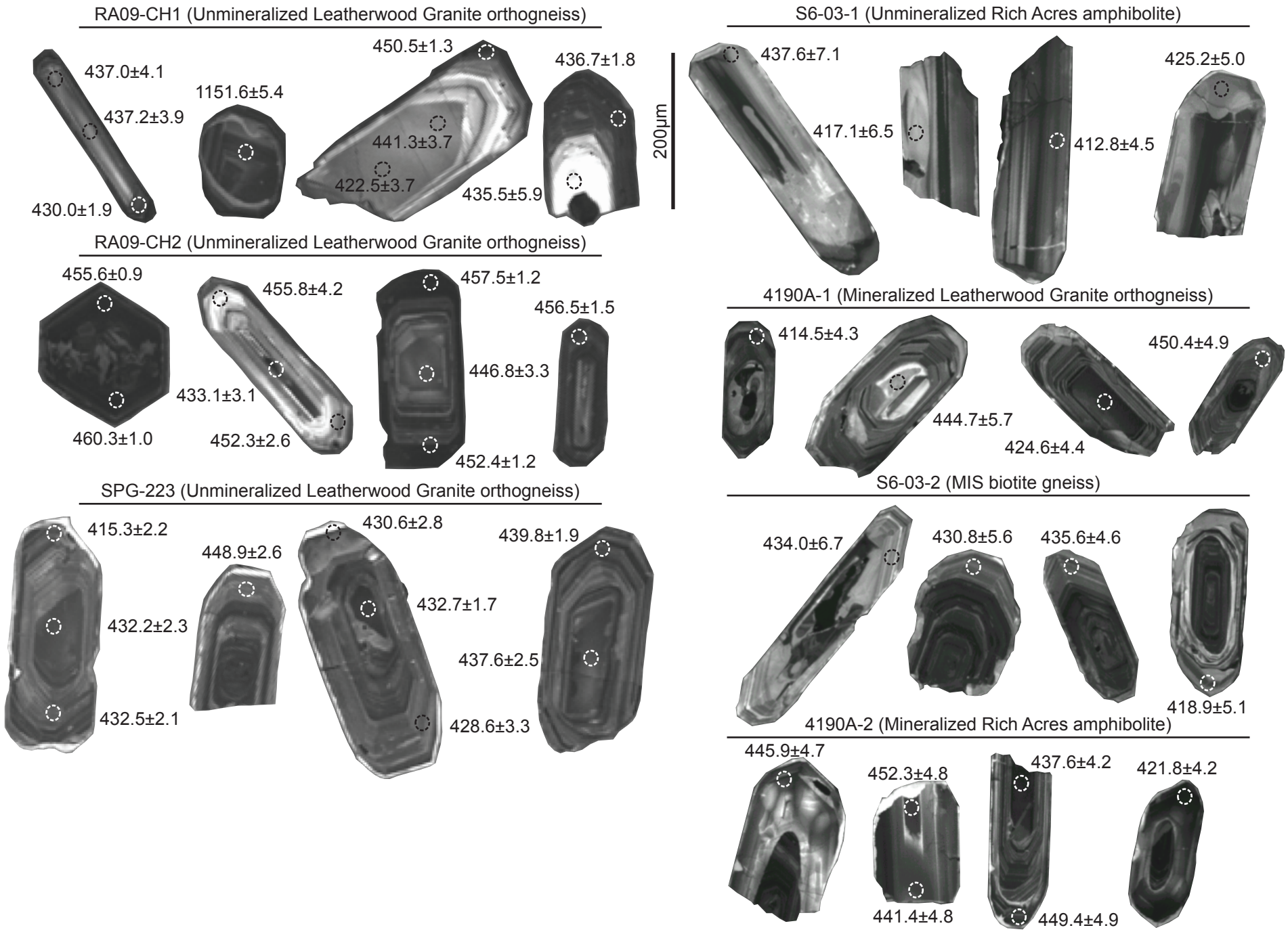
RA09-CH1 (Unmineralized Leatherwood Granite orthogneiss)
437.0±4.1
437.2±3.9
430.0±1.9
1151.6±5.4
450.5±1.3
441.3±3.7
422.5±3.7
435.5±5.9
436.7±1.8
200µm
RA09-CH2 (Unmineralized Leatherwood Granite orthogneiss)
455.6±0.9
460.3±1.0
455.8±4.2
433.1±3.1
452.3±2.6
457.5±1.2
446.8±3.3
452.4±1.2
456.5±1.5
SPG-223 (Unmineralized Leatherwood Granite orthogneiss)
415.3±2.2
432.2±2.3
432.5±2.1
448.9±2.6
430.6±2.8
432.7±1.7
437.6±2.5
428.6±3.3
439.8±1.9
S6-03-1 (Unmineralized Rich Acres amphibolite)
437.6±7.1
417.1±6.5
412.8±4.5
425.2±5.0
4190A-1 (Mineralized Leatherwood Granite orthogneiss)
414.5±4.3
444.7±5.7
424.6±4.4
450.4±4.9
S6-03-2 (MIS biotite gneiss)
434.0±6.7
430.8±5.6
435.6±4.6
418.9±5.1
4190A-2 (Mineralized Rich Acres amphibolite)
445.9±4.7
452.3±4.8
441.4±4.8
437.6±4.2
449.4±4.9
421.8±4.2

Figure 3

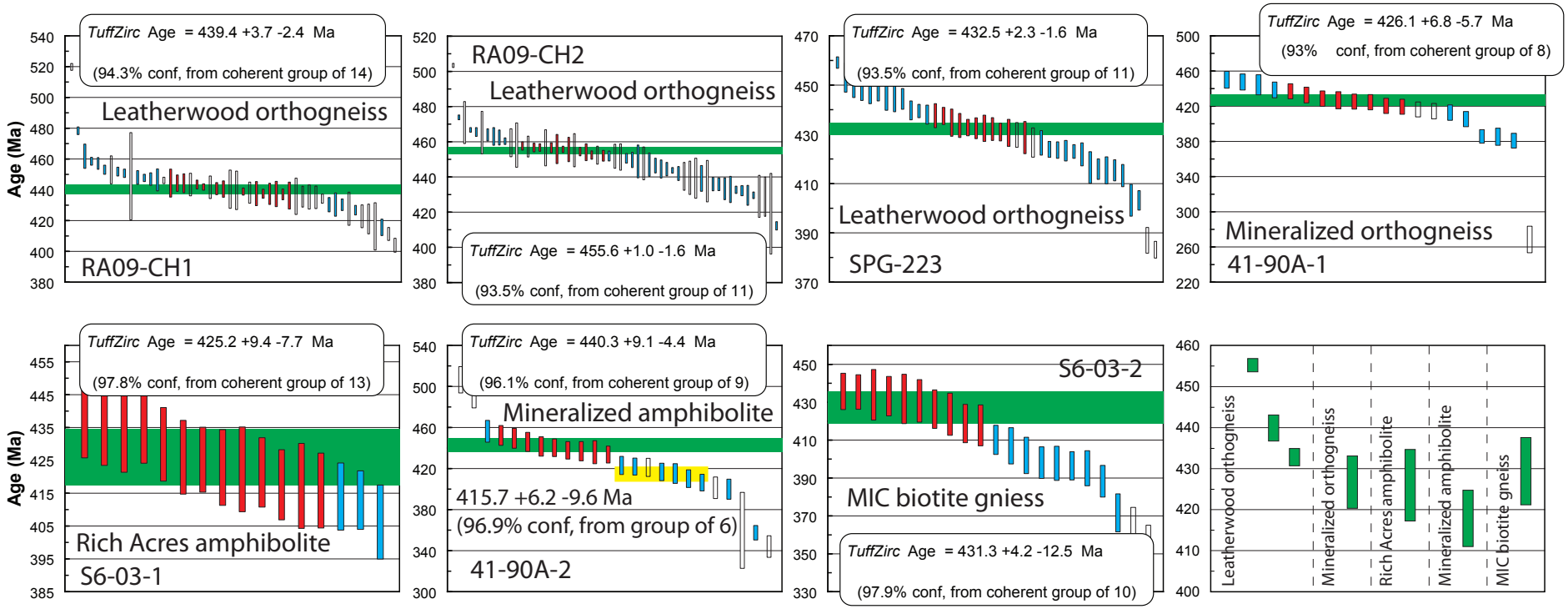
TuffZirc Age = 439.4 +3.7 -2.4 Ma
(94.3% conf, from coherent group of 14)
Leatherwood orthogneiss
RA09-CH1
Age (Ma)
RA09-CH2
Leatherwood orthogneiss
TuffZirc Age = 455.6 +1.0 -1.6 Ma
(93.5% conf, from coherent group of 11)
TuffZirc Age = 432.5 +2.3 -1.6 Ma
(93.5% conf, from coherent group of 11)
Leatherwood orthogneiss
SPG-223
TuffZirc Age = 426.1 +6.8 -5.7 Ma
(93% conf, from coherent group of 8)
Mineralized orthogneiss
41-90A-1
TuffZirc Age = 425.2 +9.4 -7.7 Ma
(97.8% conf, from coherent group of 13)
Rich Acres amphibolite
S6-03-1
Age (Ma)
TuffZirc Age = 440.3 +9.1 -4.4 Ma
(96.1% conf, from coherent group of 9)
Mineralized amphibolite
415.7 +6.2 -9.6 Ma
(96.9% conf, from group of 6)
41-90A-2
S6-03-2
MIC biotite gniess
TuffZirc Age = 431.3 +4.2 -12.5 Ma
(97.9% conf, from coherent group of 10)
Leatherwood orthogneiss
Mineralized orthogneiss
Rich Acres amphibolite
Mineralized amphibolite
MIC biotite gneiss

Figure 4

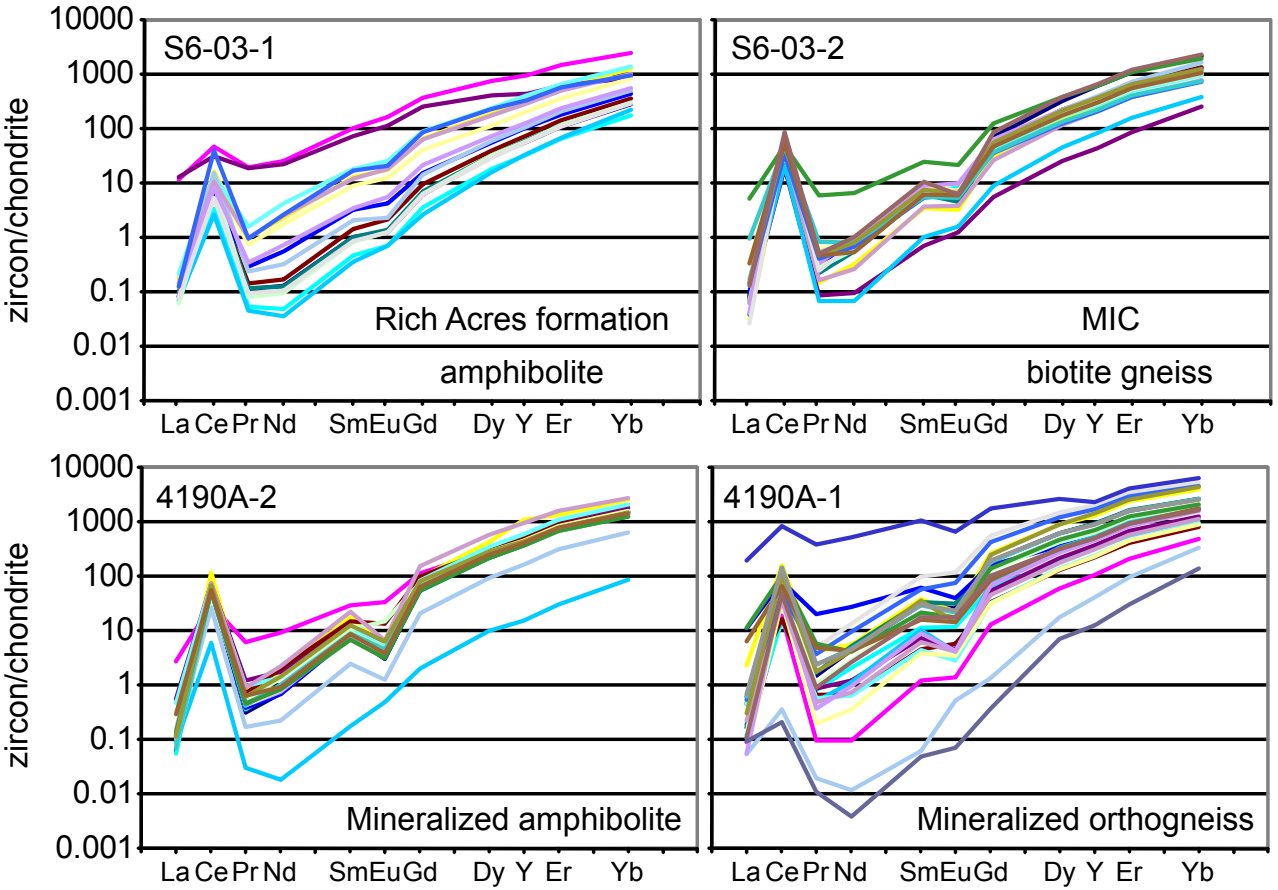
S6-03-1
Rich Acres formation
amphibolite
S6-03-2
MIC
biotite gneiss
4190A-2
Mineralized amphibolite
4190A-1
Mineralized orthogneiss
zircon/chondrite
10000
1000
100
10
1
0.1
0.01
0.001
La Ce Pr Nd Sm Eu Gd Dy Y Er Yb

Figure 5

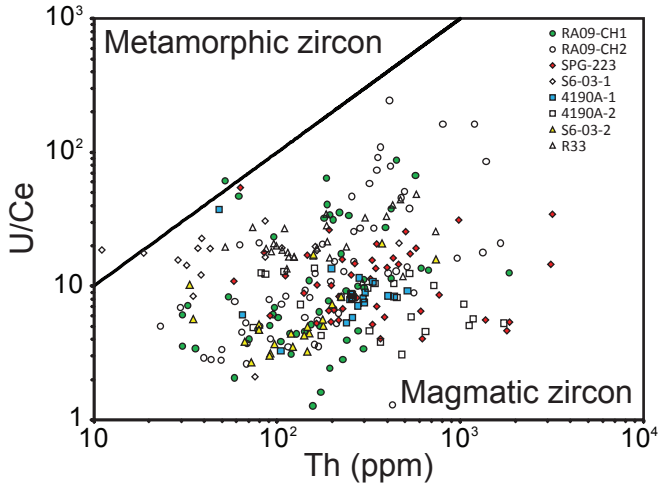
Metamorphic zircon
Magmatic zircon
RA09-CH1
RA09-CH2
SPG-223
S6-03-1
4190A-1
4190A-2
S6-03-2
R33
U/Ce
Th (ppm)
1
10
10²
10³
10⁴

Supplemental material: Concordia diagrams

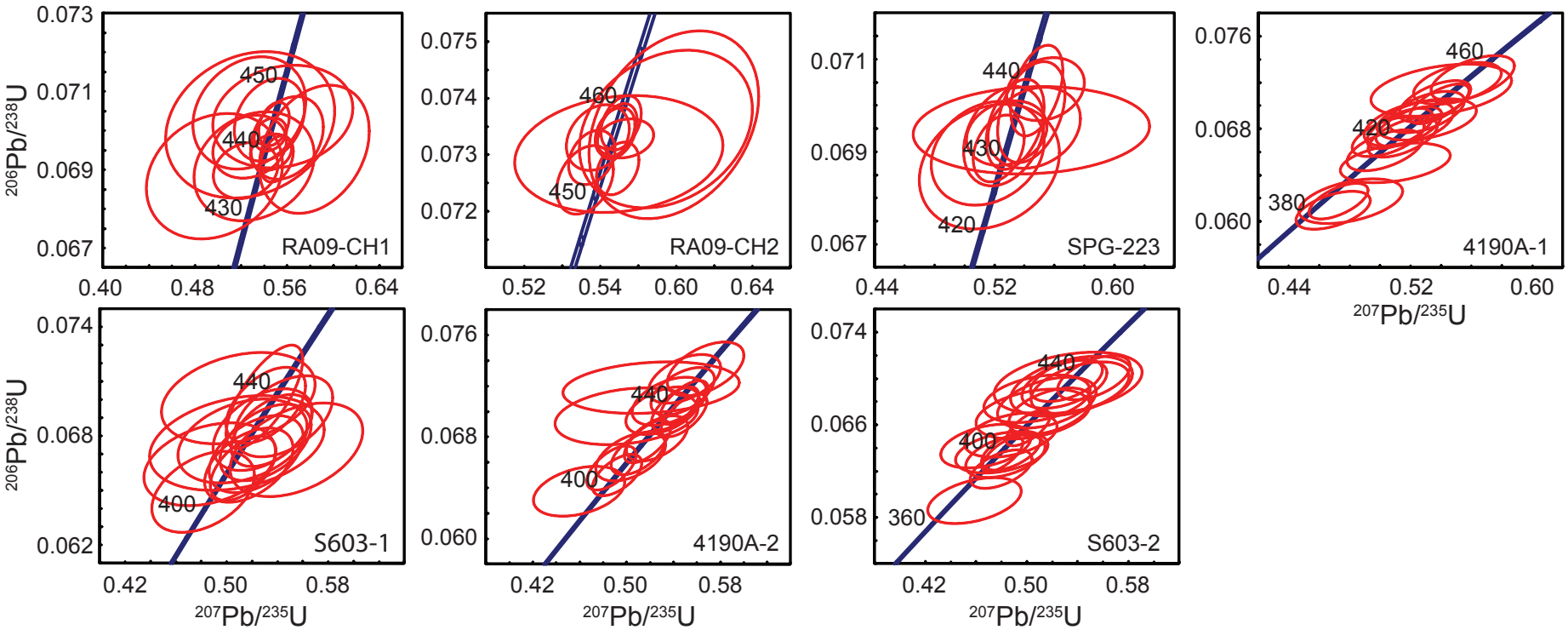

TABLE 1: U-Th-Pb SHRIMP analytical data for zircons from the MIC

Zircon. spot	Common ^{206}Pb (%)[1]	U (ppm)	Th (ppm)	$^{232}Th/^{238}Pb$	^{207}Pb Corr.[2] $^{206}Pb/^{238}U$ age[3] (Ma)	Error (abs) (My)	$^{207}Pb/^{235}U$	Error (%)	$^{206}Pb/^{238}U$	Error (%)	Error Corr.	^{204}Pb Corr.[2] $^{207}Pb/^{206}Pb$ age[3] (Ma)	Error (abs.) (My)	Discor-dant (%)
RA09-CH1 Leatherwood Granite orthogneiss														
R1-1.1	0.06	280	275	1.01	430.1	2.3	0.5449	1.6616	0.0691	0.544	0.327	497.8	34.6	16
R1-1.2	2.73	138	96	0.72	437.9	3.4	0.3495	18.2183	0.0687	1.102	0.061	-564.1	490.6	-232
R1-1.3	0.55	114	173	1.57	437.2	3.9	0.4969	4.8564	0.0698	0.937	0.193	267.9	109.3	-38
R1-2.1	0.20	453	276	0.63	430.0	1.9	0.5227	1.7228	0.0689	0.447	0.260	411.9	37.2	-4
R1-2.3	-0.23	151	228	1.56	437.0	4.1	0.5834	3.3521	0.0705	0.948	0.283	603.5	69.6	37
R1-3.1	0.40	2077	218	0.11	520.0	1.1	0.7108	1.1179	0.0844	0.235	0.210	643.2	23.5	23
R1-3.2	2.46	359	149	0.43	411.0	2.1	0.4674	5.4092	0.0656	0.586	0.108	272.5	123.2	-33
R1-4.1	0.00	154	191	1.28	461.6	4.0	0.5880	2.4407	0.0743	0.861	0.353	505.6	50.2	9
R1-5.1	1.24	54	58	1.12	427.4	5.4	0.4710	9.3554	0.0681	1.364	0.146	202.5	214.8	-52
R1-5.2	7.07	1255	239	0.20	415.9	7.7	0.4438	42.6347	0.0661	1.788	0.042	132.6	1001.6	-68
R1-6.1	1.01	87	104	1.23	436.0	4.4	0.4846	8.4200	0.0695	1.114	0.132	220.3	193.1	-49
R1-6.2	1.32	91	101	1.15	452.8	4.6	0.4700	8.5470	0.0720	1.108	0.130	66.9	201.7	-85
R1-6.3	0.93	129	91	0.73	443.2	3.7	0.4758	6.2656	0.0706	0.900	0.144	143.0	145.5	-67
R1-7.1	0.16	346	96	0.29	1151.6	5.4	2.0850	1.2447	0.1954	0.475	0.382	1131.3	22.9	-2
R1-8.1	0.63	1832	1848	1.04	438.6	1.2	0.5456	1.3392	0.0705	0.269	0.201	459.1	29.1	5
R1-8.2	1.40	2915	568	0.20	478.3	1.2	0.6059	4.0364	0.0771	0.312	0.077	492.9	88.7	3
R1-9.1	0.03	1105	186	0.17	1027.4	2.4	1.7745	0.5453	0.1730	0.237	0.435	1052.3	9.9	2
R1-10.1	1.47	122	119	1.01	434.9	3.7	0.4440	7.5998	0.0690	0.935	0.123	31.4	180.7	-93
R1-11.1	0.45	178	296	1.71	444.0	3.1	0.5560	4.4760	0.0714	0.750	0.168	472.4	97.6	6
R1-12.1	1.15	140	95	0.70	435.3	3.4	0.4573	5.9299	0.0692	0.846	0.143	95.7	138.9	-78
R1-13.1	0.00	382	52	0.14	440.2	2.7	0.5598	2.2973	0.0708	0.610	0.265	504.4	48.7	14
R1-14.1	0.57	60	33	0.56	420.7	4.8	0.4719	5.6038	0.0671	1.182	0.211	241.8	126.2	-42
R1-14.2	0.02	614	194	0.33	437.2	1.5	0.5510	1.0667	0.0703	0.343	0.322	485.9	22.3	11
R1-14.3	0.15	667	180	0.28	434.0	1.5	0.5553	1.4148	0.0698	0.336	0.238	517.9	30.2	19
R1-15.1	3.59	38	30	0.82	435.5	5.9	0.2924	39.3943	0.0678	1.986	0.050	-1034.0	1175.3	-344
R1-15.2	0.30	488	223	0.47	436.7	1.8	0.5237	2.1844	0.0700	0.419	0.192	382.6	48.2	-12
R1-16.1	4.30	442	204	0.48	403.5	2.3	0.4652	14.7513	0.0644	1.030	0.070	302.2	335.5	-25
R1-17.1	0.67	1349	187	0.14	458.3	1.3	0.5711	2.1217	0.0737	0.290	0.137	460.5	46.6	0
R1-17.2	0.12	1394	446	0.33	441.5	1.0	0.5452	1.0518	0.0709	0.243	0.231	443.2	22.8	0
R1-18.1	0.03	575	296	0.53	456.9	1.9	0.5587	1.3102	0.0734	0.421	0.321	421.2	27.7	-8
R1-19.1	1.72	530	298	0.58	446.7	2.0	0.5231	4.1501	0.0715	0.518	0.125	331.1	93.4	-26
R1-20.1	0.34	943	390	0.43	451.6	1.5	0.5581	1.6067	0.0725	0.335	0.209	444.0	34.9	-2
R1-21.1	0.55	44	36	0.84	440.1	6.3	0.5298	9.4029	0.0706	1.529	0.163	390.5	208.2	-11
R1-22.1	7.46	68	78	1.19	448.6	14.3	0.6973	47.8890	0.0733	3.074	0.064	899.9	985.6	97
R1-23.1	0.42	143	169	1.23	446.1	3.6	0.5271	3.8037	0.0715	0.822	0.216	350.2	83.9	-21
R1-24.1	0.26	2158	610	0.29	445.9	1.0	0.5886	1.2882	0.0719	0.221	0.172	579.7	27.6	29
R2-1.1	12.04	99	117	1.22	422.5	3.7	0.3990	40.9540	0.0667	2.282	0.056	-147.4	1014.0	-135
R2-1.2	1.60	110	140	1.31	441.3	3.7	0.4883	10.1663	0.0704	1.027	0.101	209.4	234.5	-52
R2-1.3	0.11	951	245	0.27	450.5	1.3	0.5585	1.0521	0.0724	0.301	0.286	450.8	22.4	0
R2-2.1	0.48	135	171	1.31	437.1	3.4	0.5313	4.0173	0.0701	0.812	0.202	411.2	88.0	-6
R2-3.1	0.00	816	668	0.85	443.1	1.4	0.5485	0.9786	0.0712	0.322	0.329	448.2	20.5	1
R2-3.2	0.38	381	237	0.64	440.5	2.0	0.5271	2.4836	0.0706	0.462	0.186	377.6	54.9	-14
R2-4.1	0.87	98	54	0.57	435.1	4.0	0.4609	7.1427	0.0692	0.972	0.136	114.0	167.0	-74

R2-5.1	0.05	380	62	0.17	1114.6	5.3	2.2101	1.6313	0.1905	0.460	0.282	1295.6	30.4	15
R2-5.2	0.18	1186	418	0.36	447.5	1.2	0.5562	0.9893	0.0719	0.272	0.275	456.3	21.1	2
R2-5.3	0.98	758	417	0.57	426.4	1.6	0.5326	3.8659	0.0685	0.398	0.103	468.5	85.1	10
R2-6.1	0.38	328	156	0.49	447.8	2.3	0.5473	2.3696	0.0719	0.521	0.230	421.3	51.6	-6
R2-6.2	1.42	199	193	1.00	415.2	2.7	0.4962	6.0491	0.0664	0.746	0.123	377.5	135.0	-9
R2-7.1	0.78	108	128	1.22	430.1	3.8	0.5386	5.1126	0.0691	0.926	0.181	473.8	111.2	10
R2-7.2	0.09	221	153	0.71	444.1	2.7	0.5443	2.2867	0.0713	0.607	0.266	428.0	49.2	-4
R2-8.1	0.67	77	70	0.94	444.1	4.6	0.5278	5.6740	0.0711	1.074	0.189	362.9	125.6	-18
R2-9.1	-0.31	40	30	0.78	439.4	6.3	0.5803	5.1597	0.0709	1.450	0.281	581.4	107.5	32
R2-9.2	0.04	745	201	0.28	452.8	1.5	0.5588	1.0316	0.0727	0.329	0.319	440.9	21.8	-3
RA09-CH2 Leatherwood Granite orthogneiss														
R1-1.1	1.58	64	64	1.03	439.4	4.7	0.4441	11.4998	0.0697	1.238	0.108	8.0	275.2	-98
R1-1.2	0.17	458	205	0.46	441.8	2.0	0.5356	1.6227	0.0709	0.462	0.285	405.2	34.8	-8
R1-2.1	1.44	121	111	0.95	432.7	3.8	0.5004	6.9018	0.0692	0.963	0.140	306.4	155.7	-29
R1-2.2	-0.04	458	196	0.44	435.7	1.8	0.5676	1.2844	0.0702	0.418	0.325	554.0	26.5	27
R1-3.1	0.44	258	215	0.86	444.4	2.6	0.5263	3.5611	0.0712	0.619	0.174	355.5	79.2	-20
R1-3.2	0.78	105	114	1.12	440.2	4.0	0.4876	5.7415	0.0702	0.956	0.167	211.8	131.2	-52
R1-4.1	1.36	42	40	0.97	428.8	6.0	0.4309	13.3508	0.0680	1.559	0.117	-4.1	319.9	-101
R1-4.2	1.20	50	49	1.02	439.1	5.7	0.4242	12.9995	0.0695	1.453	0.112	-96.5	317.2	-122
R1-5.1	18.30	173	211	1.26	418.8	11.5			0.0645	3.574				
R1-5.2	0.20	688	556	0.84	439.0	3.7	0.5626	4.1832	0.0707	0.803	0.192	520.5	90.1	18
R1-6.1	0.05	1441	511	0.37	429.3	0.9	0.5364	0.8376	0.0689	0.221	0.264	469.2	17.9	9
R1-6.2	0.05	2619	527	0.21	443.6	0.8	0.5538	0.6413	0.0713	0.180	0.281	466.3	13.6	5
R1-7.1	-0.07	207	105	0.53	429.3	2.8	0.5470	2.1781	0.0690	0.657	0.302	509.3	45.7	18
R1-8.1	0.04	1694	354	0.22	457.5	1.2	0.5710	0.7564	0.0736	0.266	0.352	463.9	15.7	1
R1-8.2	-0.10	168	142	0.87	446.8	3.3	0.5770	3.2362	0.0720	0.738	0.228	535.3	69.0	19
R1-8.3	0.02	1481	415	0.29	452.4	1.2	0.5691	0.7946	0.0728	0.260	0.327	481.1	16.6	6
R1-9.1	0.35	141	168	1.22	459.4	4.0	0.5341	3.9135	0.0735	0.885	0.226	314.6	86.7	-31
R1-9.2	0.17	100	80	0.83	455.1	4.7	0.6071	3.6118	0.0735	1.038	0.287	600.4	74.9	31
R1-10.1	0.04	897	255	0.29	452.0	1.5	0.5520	1.1042	0.0726	0.343	0.310	419.4	23.4	-7
R1-10.2	0.01	1366	350	0.26	465.5	1.3	0.5850	0.8153	0.0749	0.273	0.335	477.4	17.0	3
R1-10.3	-0.46	77	68	0.92	456.5	5.2	0.6259	4.9976	0.0739	1.171	0.234	655.0	104.2	43
R1-10.4	0.06	1183	318	0.28	454.4	1.2	0.5556	0.8947	0.0730	0.269	0.300	422.0	19.1	-7
R1-10.5	0.45	986	446	0.47	411.8	1.2	0.5025	1.4956	0.0660	0.299	0.200	421.5	32.7	2
R1-11.1	0.40	9470	801	0.09	503.6	0.6	0.6306	0.9717	0.0812	0.123	0.127	466.3	21.3	-7
R1-12.1	0.03	409	176	0.44	435.8	2.0	0.5389	1.8965	0.0700	0.443	0.233	447.2	41.0	3
R1-12.2	0.11	749	284	0.39	432.0	1.4	0.5291	1.3044	0.0693	0.334	0.256	427.3	28.1	-1
R1-13.1	3.01	845	403	0.49	451.7	1.4	0.5560	4.1997	0.0725	0.411	0.098	435.5	93.1	-4
R1-13.2	2.22	487	262	0.56	444.3	1.9	0.5600	5.0753	0.0714	0.531	0.105	485.7	111.4	9
R1-13.3	0.04	1398	958	0.71	456.6	1.2	0.5690	0.7559	0.0734	0.274	0.362	460.9	15.6	1
R1-14.1	1.84	61	50	0.84	447.6	4.7	0.4131	13.9055	0.0707	1.250	0.090	-204.6	347.3	-146
R1-15.1	0.05	1172	494	0.44	432.5	1.0	0.5343	0.7951	0.0694	0.239	0.301	445.5	16.9	3
R1-15.2	0.07	1167	474	0.42	450.5	1.4	0.5552	0.9185	0.0724	0.305	0.332	438.3	19.3	-3
R1-15.3	0.03	1909	366	0.20	456.6	1.1	0.5677	0.7445	0.0734	0.241	0.324	456.2	15.6	0
R1-16.1	0.03	3952	1379	0.36	473.9	0.7	0.5916	0.4525	0.0763	0.146	0.323	462.7	9.5	-2
R1-17.1	0.04	537	261	0.50	462.4	2.1	0.5702	1.2822	0.0743	0.458	0.357	438.4	26.7	-5
R1-18.1	0.63	75	68	0.94	448.8	4.7	0.5113	5.3301	0.0717	1.075	0.202	272.6	119.6	-39
R1-19.1	0.03	4025	1194	0.31	463.9	1.8	0.5744	0.6404	0.0746	0.386	0.603	447.2	11.4	-4
R1-20.1	0.24	441	231	0.54	446.4	2.1	0.5429	1.7606	0.0716	0.484	0.275	411.4	37.9	-8

R1-21.1	-0.28	128	67	0.54	455.5	3.5	0.5944	3.1151	0.0735	0.777	0.250	555.7	65.8	22
R1-22.1	0.49	1156	425	0.38	449.6	2.2	0.5545	1.4511	0.0722	0.503	0.347	440.1	30.3	-2
R1-23.1	0.53	3762	410	0.11	466.7	0.7	0.5789	0.8121	0.0750	0.146	0.180	450.4	17.7	-3
R2-1.1	2.05	42	23	0.57	458.1	6.3	0.3615	19.0216	0.0719	1.596	0.084	-595.8	514.8	-233
R2-2.1	0.16	139	62	0.46	1190.9	7.6	2.2464	1.6967	0.2030	0.657	0.388	1203.0	30.8	1
R2-3.1	1.10	288	79	0.29	454.0	2.4	0.5696	3.9186	0.0730	0.579	0.148	475.3	85.7	5
R2-4.1	0.14	2198	1657	0.78	455.6	0.9	0.5731	1.0640	0.0733	0.193	0.181	480.6	23.1	5
R2-4.2	0.02	1850	1326	0.74	460.3	1.0	0.5717	0.7552	0.0740	0.211	0.280	453.7	16.1	-1
R2-5.1	0.96	114	151	1.37	451.2	3.8	0.4569	6.4391	0.0716	0.894	0.139	10.6	153.4	-98
R2-5.2	0.00	49	44	0.92	470.9	6.0	0.6003	3.7912	0.0759	1.281	0.338	506.4	78.5	7
R2-6.1	0.49	184	166	0.93	457.2	3.0	0.5260	3.4465	0.0731	0.674	0.196	292.3	77.2	-36
R2-6.2	-0.50	141	141	1.04	451.7	3.4	0.6097	3.9321	0.0730	0.771	0.196	624.2	83.1	37
R2-7.1	0.78	49	30	0.63	428.6	5.6	0.4329	12.1108	0.0680	1.454	0.120	7.6	289.4	-98
R2-7.2	-0.08	358	161	0.46	463.0	2.5	0.5819	1.7177	0.0745	0.545	0.317	477.5	36.0	3
R2-8.1	1.11	75	59	0.80	437.5	5.9	0.4429	13.1376	0.0694	1.446	0.110	12.3	314.0	-97
R2-8.2	0.75	77	91	1.23	465.3	6.1	0.5138	12.8959	0.0743	1.506	0.117	203.1	297.3	-56
R2-9.1	-0.27	171	90	0.55	455.8	4.2	0.5987	3.0330	0.0735	0.922	0.304	569.0	62.9	24
R2-9.2	0.34	155	160	1.06	433.1	3.1	0.5190	4.2660	0.0694	0.759	0.178	381.2	94.4	-12
R2-9.3	0.40	296	151	0.53	452.3	2.6	0.5100	3.0675	0.0723	0.587	0.191	249.5	69.3	-45
R2-10.1	0.14	750	336	0.46	456.5	1.5	0.5588	1.2067	0.0733	0.324	0.269	423.7	25.9	-7
SPG-223 Leatherwood Granite orthogneiss														
1.1	0.29	491	264	0.56	421.8	2.4	0.5297	2.8541	0.0677	0.592	0.207	480.0	61.7	14
2.1	0.58	1137	1789	1.63	432.7	1.7	0.5280	2.0753	0.0694	0.413	0.199	419.5	45.4	-3
2.2	0.71	295	164	0.58	428.6	3.3	0.5165	3.6949	0.0687	0.803	0.217	393.5	80.9	-8
2.3	0.43	268	85	0.33	430.6	2.8	0.5155	2.9850	0.0690	0.668	0.224	379.9	65.4	-12
3.1	0.18	304	145	0.49	416.4	3.2	0.5203	2.3780	0.0668	0.789	0.332	470.4	49.6	13
4.1	0.64	486	322	0.68	415.3	2.8	0.4813	3.3087	0.0663	0.697	0.211	312.3	73.6	-25
5.1	0.69	425	344	0.84	403.1	3.3	0.5061	3.2434	0.0647	0.842	0.260	481.7	69.2	19
6.1	0.02	5446	3173	0.60	481.0	0.7	0.5983	0.3630	0.0774	0.151	0.417	454.7	7.3	-5
7.1	0.05	315	197	0.65	448.9	2.6	0.5517	1.5150	0.0721	0.581	0.384	432.7	31.2	-4
8.1	-0.02	343	330	1.00	437.6	2.5	0.5483	1.2980	0.0703	0.568	0.438	473.8	25.8	8
8.2	0.05	579	458	0.82	439.8	1.9	0.5562	1.0588	0.0707	0.441	0.416	493.3	21.2	12
9.1	0.17	741	348	0.48	423.8	1.6	0.5180	1.1525	0.0680	0.392	0.340	423.5	24.2	0
10.1	0.22	330	203	0.64	453.2	3.0	0.5486	2.0134	0.0727	0.673	0.334	400.9	42.5	-11
11.1	0.12	1020	1368	1.39	423.0	1.4	0.5189	1.1135	0.0678	0.340	0.305	431.7	23.6	2
12.1	0.54	250	139	0.57	445.0	2.9	0.5336	3.5486	0.0713	0.692	0.195	381.4	78.2	-14
13.1	0.22	459	110	0.25	403.0	2.0	0.4826	1.7063	0.0645	0.508	0.298	383.1	36.6	-5
14.1	6.33	811	763	0.97	264.8	1.2	0.3185	6.5144	0.0421	0.580	0.089	406.5	145.2	53
15.1	1.42	217	91	0.43	426.7	3.0	0.4453	5.3991	0.0678	0.767	0.142	81.8	126.8	-81
15.2	0.41	464	365	0.81	423.3	2.1	0.5197	2.1535	0.0679	0.509	0.237	433.2	46.6	2
15.3	0.01	267	63	0.24	434.8	2.8	0.5446	1.6946	0.0699	0.641	0.378	473.7	34.7	9
16.1	0.78	550	618	1.16	382.9	1.7	0.4554	2.4461	0.0612	0.473	0.193	371.0	54.0	-3
17.1	4.71	1936	1851	0.99	199.8	0.6	0.2398	3.7538	0.0317	0.370	0.099	408.9	83.6	103
18.1	0.31	679	428	0.65	437.5	1.7	0.5540	1.9180	0.0704	0.397	0.207	495.6	41.4	13
19.1	0.34	250	163	0.68	386.7	2.6	0.4519	2.7930	0.0617	0.698	0.250	333.2	61.3	-14
20.1	0.09	311	216	0.72	433.6	2.5	0.5337	1.4791	0.0696	0.573	0.387	437.5	30.4	1
20.2	0.03	1158	977	0.87	439.5	1.3	0.5450	0.8231	0.0706	0.311	0.378	452.3	16.9	3
20.3	0.43	730	606	0.86	423.5	1.7	0.5133	1.5817	0.0679	0.407	0.257	406.3	34.2	-4
21.1	0.32	308	190	0.64	429.8	2.5	0.5006	2.1779	0.0687	0.604	0.278	321.4	47.5	-25

22.1	0.11	1563	3108	2.05	459.3	1.2	0.5613	0.6972	0.0738	0.260	0.373	420.1	14.4	-8
23.1	2.66	456	226	0.51	415.3	2.2	0.5430	4.3853	0.0669	0.584	0.133	563.7	94.7	35
23.2	0.89	504	397	0.81	432.2	2.3	0.5445	5.9172	0.0695	0.554	0.094	486.0	130.0	12
23.3	0.79	429	348	0.84	432.5	2.1	0.5465	2.2996	0.0695	0.516	0.224	491.9	49.4	14
24.1	0.14	322	216	0.70	447.7	2.6	0.5385	1.7170	0.0718	0.586	0.341	388.0	36.2	-13
25.1	0.11	414	191	0.48	413.1	2.3	0.5127	1.8214	0.0663	0.562	0.308	456.6	38.4	10
26.1	0.20	695	571	0.85	430.9	1.8	0.5227	1.3313	0.0691	0.428	0.322	407.1	28.2	-5
27.1	0.26	423	271	0.66	415.8	2.1	0.5112	1.7414	0.0667	0.514	0.295	437.0	37.0	5
28.1	0.27	456	252	0.57	449.4	2.2	0.5350	1.9107	0.0720	0.509	0.267	365.6	41.5	-18
29.1	0.14	860	501	0.60	446.9	1.6	0.5522	1.2130	0.0718	0.368	0.304	444.2	25.7	-1
30.1	0.13	521	329	0.65	444.5	2.1	0.5447	1.3494	0.0713	0.482	0.357	427.3	28.1	-4
31.1	0.22	303	196	0.67	445.5	2.9	0.5505	2.2257	0.0716	0.657	0.295	444.3	47.3	0
32.1	0.16	663	530	0.83	438.1	1.9	0.5294	1.4108	0.0702	0.450	0.319	398.8	30.0	-9
33.1	-0.04	107	58	0.56	1042.9	9.1	1.8239	1.5660	0.1759	0.891	0.569	1074.4	25.9	3
34.1	0.15	398	384	1.00	426.5	2.5	0.5356	1.7434	0.0685	0.600	0.344	479.9	36.2	12
34.2	0.23	353	227	0.66	432.4	2.7	0.5263	2.0888	0.0693	0.633	0.303	414.1	44.5	-4
S6-03-1 Rich Acres Formation amphibolite														
1.1	0.00	129	42	0.34	429.8	5.6	0.5449	2.8951	0.0691	1.325	0.458	498.9	56.7	16
2.1	0.09	862	507	0.61	230.9	2.9	0.2834	1.8580	0.0367	1.254	0.675	452.1	30.4	95
3.1	0.52	75	25	0.35	438.3	6.3	0.5091	4.8559	0.0701	1.462	0.301	314.9	105.3	-28
4.1	0.00	269	184	0.71	437.6	7.1	0.5296	2.3120	0.0702	1.655	0.716	401.7	36.2	-8
5.1	0.49	56	12	0.22	422.2	6.5	0.5080	5.5465	0.0676	1.571	0.283	391.0	119.4	-7
6.1	0.50	786	88	0.12	76.6	7.0	0.0870	10.0913	0.0120	9.135	0.905	305.9	97.7	297
7.1	0.00	111	40	0.37	421.3	5.3	0.5306	2.7688	0.0677	1.271	0.459	486.4	54.3	15
8.1	0.00	93	32	0.35	425.9	5.6	0.5283	3.0323	0.0684	1.339	0.442	454.3	60.4	7
9.1	0.34	82	36	0.45	422.8	5.8	0.5125	4.0628	0.0677	1.391	0.343	406.9	85.4	-4
10.1	0.00	55	10	0.18	417.1	6.5	0.5548	3.8436	0.0672	1.568	0.408	598.0	76.0	43
11.1	0.00	250	182	0.75	412.8	4.5	0.5129	2.0668	0.0662	1.100	0.533	459.3	38.8	11
12.1	0.00	162	47	0.30	425.2	5.0	0.5352	2.4094	0.0683	1.185	0.492	484.7	46.3	14
13.1	0.00	130	82	0.65	413.8	5.1	0.5171	2.7524	0.0664	1.256	0.457	470.8	54.2	14
14.1	0.00	116	39	0.34	417.5	5.4	0.5231	2.8849	0.0670	1.298	0.450	476.2	57.0	14
15.1	0.00	180	118	0.68	434.5	5.2	0.5306	2.4101	0.0697	1.225	0.508	420.9	46.3	-3
16.1	0.39	87	41	0.49	415.7	5.7	0.4864	4.3630	0.0664	1.403	0.322	332.8	93.7	-20
17.1	0.00	85	21	0.25	406.0	5.7	0.4813	3.4282	0.0649	1.407	0.410	361.4	70.5	-11
18.1	0.29	75	84	1.15	434.6	6.6	0.4979	4.2801	0.0694	1.551	0.362	285.9	91.2	-34
4190A-1 Mineralized Leatherwood Granite orthogneiss[4]														
1.1	0.16	352	217	0.64	267.7	7.6	0.3255	3.6029	0.0426	2.867	0.796	429.5808	48.6555	60
3.1	-0.10	418	284	0.70	416.5	4.3	0.5262	1.9817	0.0669	1.047	0.528	493.3261	37.0977	18
4.1	0.12	542	439	0.84	419.5	4.3	0.5148	1.7955	0.0673	1.041	0.580	432.5710	32.5951	3
5.1	0.00	315	269	0.88	412.9	4.4	0.5031	2.0145	0.0662	1.091	0.542	418.5586	37.8237	1
6.1	0.18	398	284	0.74	428.7	4.4	0.5307	2.5014	0.0688	1.057	0.423	449.8855	50.3522	5
7.1	0.05	505	309	0.63	425.3	4.3	0.5189	1.7090	0.0682	1.023	0.599	420.0675	30.5595	-1
8.1	0.00	197	53	0.28	427.0	4.9	0.5190	2.3156	0.0684	1.162	0.502	411.9986	44.7908	-3
9.1	0.00	531	367	0.71	437.1	4.3	0.5389	1.4805	0.0702	0.993	0.671	440.3149	24.4255	1
10.1	0.00	487	334	0.71	385.6	3.9	0.4727	1.6704	0.0617	1.021	0.611	434.2196	29.4453	12
10.2	0.00	118	116	1.02	444.7	5.7	0.5401	3.4918	0.0713	1.292	0.370	408.4189	72.5800	-8
11.1	0.17	444	326	0.76	448.0	4.6	0.5506	2.1417	0.0719	1.038	0.485	433.1722	41.7288	-3
12.1	0.00	146	72	0.51	385.2	4.9	0.4808	2.8953	0.0617	1.287	0.445	471.0529	57.3939	22

13.1	0.08	564	481	0.88	424.6	4.4	0.5128	1.7187	0.0680	1.043	0.607	398.6263	30.6139	-6
14.1	0.08	411	286	0.72	420.4	4.3	0.5052	1.9110	0.0673	1.048	0.548	388.5833	35.8780	-7
15.1	0.00	410	281	0.71	438.7	4.5	0.5360	1.7897	0.0704	1.049	0.586	421.3740	32.3625	-4
16.1	0.00	386	284	0.76	414.5	4.3	0.5262	1.8603	0.0666	1.064	0.572	503.4572	33.5853	21
17.1	0.11	361	308	0.88	405.4	4.4	0.5100	2.8883	0.0651	1.081	0.374	485.7484	59.1298	20
17.2	0.00	378	276	0.76	380.7	4.2	0.4692	2.1318	0.0610	1.105	0.518	445.3052	40.5263	17
18.1	0.00	320	264	0.85	450.4	4.9	0.5608	2.0008	0.0724	1.101	0.550	459.6793	37.0489	2
19.1	0.10	436	330	0.78	432.9	4.5	0.5304	1.9117	0.0695	1.048	0.548	427.8606	35.6551	-1
4190A-2 Mineralized Rich Acres Formation amphibolite[4]														
1.1	0.00	206	90	0.45	456.3	5.3	0.5675	2.3501	0.0734	1.184	0.504	456.3	5.3	0
1.2	0.04	1029	1144	1.15	433.5	4.1	0.5489	1.4611	0.0697	0.972	0.666	433.5	4.1	14
2.1	0.00	175	122	0.72	401.0	5.3	0.5201	2.7648	0.0645	1.334	0.482	401.0	5.3	36
2.2	0.00	380	251	0.68	420.9	4.4	0.5305	1.9003	0.0676	1.071	0.564	420.9	4.4	16
3.1	0.24	169	94	0.57	506.8	6.4	0.5722	3.4347	0.0812	1.292	0.376	506.8	6.4	-51
4.1	0.09	375	534	1.47	445.9	4.7	0.5476	2.0245	0.0716	1.075	0.531	445.9	4.7	-3
4.2	0.10	750	378	0.52	356.9	3.5	0.4368	1.8104	0.0571	1.008	0.557	356.9	3.5	21
5.1	0.05	740	588	0.82	440.2	4.3	0.5491	1.5261	0.0707	0.998	0.654	440.2	4.3	5
6.1	0.11	383	177	0.48	422.9	4.5	0.5260	2.0307	0.0679	1.075	0.529	422.9	4.5	9
7.1	0.21	359	351	1.01	436.9	4.7	0.5309	2.4083	0.0701	1.092	0.454	436.9	4.7	-6
7.2	0.38	147	83	0.58	435.8	5.6	0.4998	4.9781	0.0696	1.303	0.262	435.8	5.6	-34
8.2	0.00	241	152	0.65	414.9	4.8	0.5035	2.4293	0.0665	1.179	0.486	414.9	4.8	-1
8.3	0.00	513	352	0.71	409.9	4.3	0.4870	1.7778	0.0656	1.071	0.603	409.9	4.3	-11
9.1	0.19	384	596	1.60	452.3	4.8	0.5493	2.2795	0.0726	1.090	0.478	452.3	4.8	-10
9.2	0.17	352	503	1.47	441.4	4.8	0.5362	2.4178	0.0708	1.094	0.453	441.4	4.8	-7
10.1	0.09	563	715	1.31	416.4	4.3	0.5099	1.8368	0.0668	1.043	0.568	416.4	4.3	3
11.1	0.81	348	408	1.21	449.4	4.9	0.5210	5.9000	0.0719	1.155	0.196	449.4	4.9	-31
11.2	0.09	956	806	0.87	437.6	4.2	0.5412	1.5262	0.0703	0.988	0.647	437.6	4.2	2
12.1	0.11	616	485	0.81	489.2	4.9	0.4956	2.1311	0.0778	1.032	0.484	489.2	4.9	-98
13.1	0.28	181	195	1.11	399.5	4.9	0.4593	3.4718	0.0637	1.255	0.362	399.5	4.9	-25
15.1	0.09	724	1293	1.84	406.0	4.1	0.4918	1.7449	0.0650	1.016	0.583	406.0	4.1	0
16.1	0.00	683	1238	1.87	421.8	4.2	0.5179	1.5646	0.0677	1.007	0.643	421.8	4.2	3
16.2	4.76	3758	1896	0.52	269.0	5.9	0.2362	46.2083	0.0420	2.359	0.051	269.0	5.9	-214
S6-03-2 MIS biotite gneiss														
1.1	0.15	292	198	0.70	435.6	4.6	0.5309	2.1829	0.0699	1.077	0.493	416.9	42.4	-4
2.1	0.13	172	86	0.52	395.1	4.7	0.4831	2.6392	0.0633	1.192	0.452	428.0	52.5	8
3.1	0.32	155	102	0.68	434.0	6.7	0.5323	4.4665	0.0696	1.565	0.350	430.3	93.2	-1
4.1	0.00	165	37	0.23	431.9	6.6	0.5350	3.6599	0.0693	1.533	0.419	451.2	73.8	4
5.1	0.00	260	166	0.66	430.8	5.6	0.5419	2.9099	0.0692	1.321	0.454	482.7	57.3	12
6.1	0.00	361	220	0.63	418.9	5.1	0.5184	2.5731	0.0672	1.228	0.477	450.3	50.2	7
7.1	0.00	256	164	0.66	435.9	4.8	0.5529	2.1128	0.0701	1.121	0.530	499.5	39.4	14
8.1	0.00	108	39	0.37	423.8	5.6	0.5155	3.0775	0.0679	1.337	0.434	414.0	62.0	-2
9.1	0.31	156	101	0.67	426.4	5.1	0.5079	3.3638	0.0683	1.224	0.364	369.3	70.6	-13
9.2	0.26	120	80	0.69	417.8	5.4	0.5047	3.6472	0.0669	1.317	0.361	399.7	76.2	-4
10.1	0.23	235	157	0.69	397.6	4.5	0.4800	3.0926	0.0636	1.151	0.372	400.6	64.3	1
11.1	0.00	658	174	0.27	598.9	5.8	0.8669	1.3364	0.0979	0.998	0.746	749.4	18.8	24
12.1	0.00	172	89	0.54	433.3	5.2	0.5295	2.5751	0.0695	1.221	0.474	422.5	50.6	-2
13.1	0.27	206	162	0.81	406.9	4.8	0.4874	3.0588	0.0651	1.203	0.393	383.2	63.2	-6
14.1	0.20	198	137	0.71	401.9	4.8	0.4676	3.1177	0.0642	1.210	0.388	322.1	65.3	-20

15.1	0.00	115	70	0.63	371.4	5.0	0.4588	3.2753	0.0594	1.364	0.417	451.4	66.1	21
16.1	0.99	158	109	0.71	365.3	4.5	0.3728	6.4210	0.0578	1.279	0.199	38.2	150.6	-89
17.1	0.08	905	411	0.47	410.2	3.9	0.5010	1.4277	0.0657	0.967	0.677	423.8	23.4	3
18.1	0.00	363	250	0.71	398.0	4.2	0.4873	1.9502	0.0638	1.073	0.550	429.9	36.3	8
19.1	0.00	298	195	0.68	388.2	4.2	0.4795	2.0729	0.0622	1.098	0.530	449.5	39.1	16
20.1	0.00	213	133	0.64	356.3	4.2	0.4288	2.5905	0.0569	1.193	0.461	398.5	51.5	12
21.1	0.08	1200	809	0.70	396.4	3.8	0.4809	1.3772	0.0634	0.963	0.699	410.9	22.0	4

All errors are presented at 1σ

[1] Negative values denote reversely discordant analyses.

[2] The model of Stacey and Kramers (1975) is used for common Pb corrections

[3] Decay constants used for age calculations are from Steiger and Jager (1977)

[4] Samples provided by the Virginia Museum of Natural History

TABLE 2: U-Th-Pb SHRIMP analytical data for zircon standard R33

Zircon. spot	Common ^{206}Pb (%)[1]	U (ppm)	Th (ppm)	$^{232}Th/^{238}Pb$	^{207}Pb Corr.[2] $^{206}Pb/^{238}U$ age[3] (Ma)	Error (abs) (My)	^{204}Pb Corr.[2] $^{207}Pb/^{206}Pb$ age[3] (Ma)	Error (abs) (My)
Standard R33- first analytical session (November 2009)								
R33-1	0.14	92	44	0.50	410.2	3.7	426.3	73.1
R33-2	0.24	202	90	0.46	412.7	4.0	370.1	54.3
R33-3	0.64	175	117	0.69	419.2	4.1	188.4	92.6
R33-4	0.25	185	118	0.66	416.8	4.0	368.4	56.2
R33-5	0.62	113	46	0.42	414.4	3.5	259.7	113.1
R33-6	0.00	129	83	0.66	395.5	3.0	453.2	49.1
R33-7	0.88	113	60	0.55	413.6	3.3	111.9	173.1
R33-8	0.52	133	94	0.73	415.8	3.3	237.6	105.2
R33-9	0.07	352	239	0.70	415.0	4.0	449.9	37.5
R33-10	-0.13	272	180	0.68	424.1	4.1	465.9	41.9
R33-11	1.10	105	47	0.47	423.0	4.1	86.3	168.4
R33-12	0.30	235	160	0.70	419.7	4.1	290.3	93.2
R33-13	0.28	307	270	0.91	420.3	4.1	314.1	56.7
R33-14	-0.24	152	98	0.66	413.7	4.0	525.3	58.4
R33-15	-0.06	222	168	0.78	411.9	5.2	532.4	39.0
R33-16	0.13	247	152	0.63	415.0	4.0	442.6	44.5
R33-17	0.31	133	71	0.55	413.4	4.0	239.8	80.1
R33-18	-0.38	180	136	0.78	423.2	3.1	578.4	74.1
R33-19	0.04	277	184	0.68	422.9	4.1	436.5	41.3
R33-20	0.21	158	81	0.53	421.6	4.1	316.3	84.3
R33-21	0.28	232	191	0.85	419.3	4.1	290.3	57.6
R33-22	-0.29	145	95	0.68	424.6	3.2	524.9	79.5
R33-23	0.21	103	46	0.47	425.6	3.7	379.0	80.6
R33-24	0.28	147	86	0.61	425.9	4.1	304.4	88.5
R33-25	0.15	107	43	0.42	432.5	3.6	320.0	79.6
R33-26	0.42	258	216	0.86	430.2	3.1	321.2	91.9
R33-27	0.54	61	23	0.39	422.3	4.3	308.3	196.7
R33-28	0.00	536	384	0.74	415.7	4.0	448.7	24.7
R33-29	0.43	155	94	0.63	413.9	3.8	251.5	80.8
R33-30	0.45	258	196	0.78	403.1	3.6	359.3	73.0
R33-31	0.48	130	65	0.52	425.1	3.7	298.1	82.8
R33-32	3.77	108	44	0.42	415.7	3.9	67.4	277.6
R33-33	0.85	83	40	0.49	413.2	4.6	183.3	147.5
R33-34	0.20	220	137	0.64	417.7	4.0	430.5	57.3
R33-35	0.32	219	160	0.76	426.7	4.1	303.1	59.1

R33-36	0.93	109	62	0.59	424.8	4.2	116.9	137.0
R33-37	2.06	63	31	0.50	415.6	5.5	-555.4	415.7
R33-38	1.10	122	78	0.66	414.4	4.1	75.8	176.8
R33-39	0.55	134	85	0.65	424.1	4.2	206.4	167.4
Standard R33- second analytical sesssion (October 2010)								
R33-1.1	0.19	150	96	0.66	404.8	3.5	334.0	71.9
R33-2.1	0.00	127	57	0.46	417.5	3.9	318.9	61.6
R33-3.1	0.08	587	432	0.76	418.1	3.9	421.0	31.7
R33-4.1	0.00	172	121	0.73	420.1	3.9	399.4	45.8
R33-5.1	0.30	172	106	0.64	415.0	3.9	312.7	73.5
R33-6.1	0.11	444	549	1.28	382.3	3.6	400.1	39.2
R33-7.1	0.38	253	135	0.55	409.0	3.8	309.3	63.6
R33-8.1	0.24	168	108	0.67	412.2	3.9	402.2	67.8
R33-9.1	0.00	1060	651	0.63	421.0	3.9	462.1	30.4
R33-10.1	0.00	170	128	0.78	412.4	3.9	499.5	49.2
R33-11.1	0.48	170	126	0.77	411.2	3.8	263.5	90.5
R33-12.1	-0.19	154	125	0.84	414.9	3.9	543.0	73.4
R33-13.1	0.27	231	215	0.96	415.7	3.9	301.9	66.9
R33-14.1	0.00	227	185	0.84	422.8	4.0	432.6	43.7
R33-15.1	0.13	294	324	1.14	420.3	3.9	420.7	43.9
R33-16.1	0.22	262	122	0.48	439.4	4.1	360.8	53.5
R33-17.1	-0.17	275	223	0.84	426.6	4.0	554.2	43.1
R33-18.1	0.00	512	344	0.69	434.5	4.1	383.0	30.1
R33-19.1	0.14	746	530	0.73	422.7	4.0	382.7	32.0
R33-20.1	0.27	327	208	0.66	416.5	3.9	408.6	62.1
R33-21.1	0.00	193	82	0.44	438.9	4.1	484.3	51.5
R33-22.1	0.18	983	833	0.87	435.8	4.1	380.9	31.1
R33-23.1	0.09	612	476	0.80	431.2	4.0	418.9	31.8
R33-24.1	0.28	290	263	0.94	410.4	3.8	334.8	60.6
R33-25.1	0.39	182	138	0.79	425.8	4.0	334.3	86.5
R33-27	0.00	191	106	0.58	427.3	4.0	426.9	53.5
R33-28	0.17	311	214	0.71	427.8	4.0	328.4	55.9
R33-29	0.46	211	176	0.86	423.1	4.0	278.9	91.8

All errors are presented at 1σ

[1] Negative values denote reversely discordant analyses.

[2] The model of Stacey and Kramers (1975) is used for common Pb corrections

[3] Decay constants used for age calculations are from Steiger and Jager (1977)

Table 3. SHRIMP Trace-element data for zircons from rocks associated with the Coles Hill uranium deposit normalized to chondrite (ppm)

Zircon.Spot	La	Ce	Nd	Sm	Eu	Gd	Dy	Y	Er	Yb	Hf
4190A-1 Mineralized Leatherwood Granite orthogneiss[1]											
1.1	0.879	25.3	5.8	5.9	2.60	30.3	97.0	867	151	306	6644
3.1	0.018	47.5	0.6	1.8	0.29	17.8	84.0	912	172	325	10668
4.1	0.181	60.1	1.1	2.4	0.49	23.4	109.7	1148	215	403	10925
5.1	0.029	52.7	1.2	3.0	1.04	26.7	101.7	1066	195	357	9519
6.1	0.039	41.7	0.5	1.5	0.26	14.6	72.0	789	148	283	10973
7.1	0.037	40.7	0.4	1.6	0.24	15.4	83.2	913	171	329	11187
8.1	0.027	5.0	0.0	0.0	0.04	0.5	3.3	33	7	19	11173
9.1	0.020	46.3	0.4	1.7	0.23	16.9	87.5	949	177	338	10917
10.1	0.150	60.3	0.9	2.2	0.38	22.9	116.5	1256	239	463	10449
10.2	0.024	33.9	0.8	2.2	1.16	20.2	78.6	815	150	293	10775
11.1	0.037	52.2	0.6	1.9	0.36	18.7	92.8	974	183	361	12250
12.1	0.033	22.2	0.1	0.5	0.10	5.6	31.0	353	68	143	11784
13.1	0.048	63.1	1.4	4.5	0.50	41.8	192.3	2035	352	612	11768
14.1	0.043	44.4	0.5	1.6	0.29	16.6	80.4	862	164	315	11560
15.1	0.038	44.3	0.5	1.7	0.29	16.6	82.8	907	168	331	11553
16.1	0.037	44.5	0.6	1.7	0.32	17.4	82.2	881	165	320	11538
17.1	0.023	46.8	0.6	1.8	0.35	17.6	79.0	842	152	298	10797
17.2	0.043	44.0	0.5	1.4	0.24	14.8	72.1	801	146	283	11714
18.1	0.036	57.3	0.9	2.6	0.49	21.6	93.2	929	173	330	11512
19.1	0.094	46.5	0.6	1.8	0.29	17.1	82.7	876	168	326	11643
S6-03-1 Rich Acres Formation amphibolite											
1.1	0.027	5.4	0.1	0.2	0.10	1.7	10.3	123	24	64	11730
2.1	3.720	38.6	16.1	20.9	12.72	100.6	251.9	2036	321	551	7008
4.1	0.056	13.4	1.5	2.6	1.35	17.5	63.5	751	130	284	7725
5.1	0.022	2.8	0.0	0.1	0.05	1.0	6.0	73	14	39	10292
6.1	4.236	26.2	13.9	14.7	8.83	69.5	135.8	940	133	195	7483
7.1	0.032	5.5	0.1	0.3	0.17	2.6	13.2	163	31	79	10212
8.1	0.032	5.6	0.1	0.2	0.11	1.9	10.7	131	26	66	11140
9.1	0.026	5.4	0.3	0.7	0.33	4.2	18.9	223	39	97	8764
10.1	0.023	2.2	0.0	0.1	0.05	0.7	5.3	73	15	50	10757
11.1	0.069	11.6	2.7	3.6	1.94	24.2	79.1	874	146	312	7542
12.1	0.020	8.0	0.1	0.2	0.10	1.7	10.7	129	25	68	12397
13.1	0.045	8.3	1.1	1.8	0.96	11.1	38.2	446	79	185	7151
14.1	0.041	12.8	0.2	0.4	0.17	3.9	19.8	234	45	111	11657
15.1	0.046	8.7	1.6	2.4	1.38	17.2	58.7	629	109	231	8384
16.1	0.027	6.9	0.4	0.7	0.43	5.9	24.2	280	52	123	8846
17.1	0.025	4.4	0.1	0.2	0.10	1.7	9.8	123	24	64	9787
18.1	0.041	33.3	1.6	3.5	1.63	23.0	76.5	714	124	213	8801
4190A-2 Mineralized Rich Acres Formation amphibolite[1]											

1.1	0.029	15.6	0.1	0.2	0.11	3.5	20.2	227	45	110	13202
1.2	0.750	133.3	3.4	7.9	1.72	71.1	293.2	2741	515	899	9925
2.1	0.039	12.6	1.3	2.3	0.90	16.7	62.3	703	121	255	10196
2.2	0.145	42.2	0.8	1.5	0.35	14.5	73.1	787	147	285	11413
3.1	0.197	13.4	0.4	0.9	0.45	9.1	43.3	475	90	180	10690
4.1	0.062	114.6	3.2	6.7	2.37	51.4	205.8	1954	355	594	10065
4.2	3.566	67.3	17.2	12.6	3.09	42.4	117.9	1125	200	375	11871
5.1	0.034	55.4	0.7	2.1	0.32	20.3	110.7	1172	220	425	12880
6.1	0.148	26.6	0.4	0.9	0.22	8.8	47.0	509	100	210	12979
7.1	0.045	74.3	1.8	4.0	1.16	34.7	141.9	1376	255	444	10497
7.2	0.018	28.3	0.2	0.8	0.26	8.4	45.5	498	98	202	12130
8.2	0.073	30.2	0.5	1.2	0.31	12.2	58.7	679	127	254	11002
8.3	0.018	48.4	0.6	1.8	0.32	18.5	90.5	988	185	359	11944
9.1	0.219	61.8	8.3	19.8	9.14	151.9	497.3	4250	747	1165	9192
9.2	0.172	40.3	6.0	11.6	5.87	115.4	404.4	3661	645	1028	8782
10.1	0.197	117.2	3.0	5.9	1.65	48.9	203.8	1903	350	590	11088
11.1	3.599	86.1	2.5	4.4	1.37	37.5	154.6	1507	275	470	8723
11.2	0.098	85.5	2.7	7.1	1.12	67.4	297.9	3051	558	994	12277
12.1	2.061	55.5	2.6	3.3	1.11	23.5	108.2	1086	205	394	13330
13.1	0.035	39.3	1.6	3.6	1.35	27.5	105.0	1085	200	363	8254
15.1	0.217	120.6	2.8	6.0	1.80	51.7	204.4	1929	346	571	10350
16.1	0.053	126.1	2.8	6.0	2.00	50.9	203.3	1969	350	585	10041
16.2	62.837	689.2	326.3	212.0	51.17	468.5	874.8	4944	889	1416	13292

S6-03-2 Fork Mtn. Formation biotite gneiss

1.1	0.022	53.9	0.5	1.7	0.55	15.7	74.1	808	151	288	10318
2.1	0.010	31.8	0.2	0.7	0.25	8.8	48.6	549	109	222	10904
3.1	0.025	46.8	0.5	1.3	0.64	14.2	73.7	767	151	305	12847
4.1	0.023	15.3	0.1	0.1	0.10	1.5	8.6	94	19	57	12891
5.1	0.026	55.3	0.4	1.4	0.56	14.7	74.5	778	150	299	12900
6.1	0.012	46.9	0.3	1.3	0.35	12.5	66.6	725	142	284	13256
7.1	0.031	47.7	0.4	1.3	0.45	13.1	61.2	686	127	256	10462
8.1	0.021	17.7	0.0	0.2	0.12	2.4	15.1	182	35	84	11694
9.1	0.022	48.3	0.4	1.2	0.49	11.6	56.0	592	110	211	10747
9.2	0.021	41.9	0.4	1.2	0.52	12.5	58.3	627	118	231	10240
10.1	0.113	50.3	0.5	1.7	0.57	14.3	64.6	682	127	246	9384
11.1	0.057	36.0	0.6	1.5	0.50	13.9	73.4	846	161	363	10782
12.1	0.020	33.7	0.2	0.7	0.29	7.2	39.7	443	83	172	11372
13.1	0.013	59.6	0.6	1.8	0.77	17.1	75.3	770	146	271	11027
14.1	0.009	51.6	0.5	1.5	0.55	14.0	61.7	665	123	232	10058
15.1	0.046	28.3	0.4	1.1	0.50	9.5	41.7	446	84	164	9385
16.1	0.306	38.9	0.5	1.1	0.41	10.0	44.2	477	90	171	7803
17.1	0.027	40.4	0.5	1.6	0.40	18.8	108.5	1316	242	486	11182
18.1	1.702	39.9	4.0	4.9	1.65	33.7	127.7	1314	236	428	9875
19.1	0.050	49.7	0.5	1.5	0.50	14.9	72.5	795	143	280	9817
20.1	0.107	44.5	0.3	1.3	0.46	12.6	59.2	644	121	233	10161

21.1	0.042	70.8	0.6	2.1	0.47	23.2	127.4	1413	263	507	11487

Notes: All reported values are normalized to chondrite using the values of Anders and Grevesse (1989) modified by Korotev (1996).

[1] Samples provided by the Virginia Museum of Natural History

Table 4. LA-ICMPS Trace-element data for zircons from the Leatherwood Granite normalized to chondrite (ppm)

Zircon.Spot	La[1]	Ce	Sm[1]	Eu[1]	Dy	Lu	Hf	Y
RA09-CH1 Leatherwood Granite orthogneiss								
R1-1.1		26.7	21.3	2.3	331.2	123.4	9317	2987
R1-1.2	0.6	19.0	4.8	0.6	102.2	54.4	9944	1005
R1-1.3		67.0	15.0	4.5	268.7	129.9	9010	2659
R1-2.1		93.2	25.7	7.4	380.2	166.4	8991	3571
R1-2.3		51.0	5.8	1.0	181.8	101.0	10724	1821
R1-3.1	15.0	55.5	34.9	7.5	165.1	215.5	13344	1567
R1-3.2	1.4	30.9	6.3	1.0	107.4	66.5	11515	1139
R1-4.1		18.9	13.9	5.2	210.3	77.1	8392	1871
R1-5.1		24.9	32.6	14.0	363.4	112.7	7336	2924
R1-5.2	127.0	302.0	44.6	11.2	309.1	156.7	12740	2723
R1-6.1		21.6	11.5	2.5	222.4	99.5	9433	2002
R1-6.2		14.8	12.5	1.9	167.5	78.5	9727	1468
R1-6.3	0.5	24.2	5.0	1.5	122.4	70.3	9892	1245
R1-7.1		14.1	2.7		119.9	61.0	10487	1231
R1-8.1	0.4	138.8	24.7	2.4	644.1	288.5	9800	6523
R1-8.2	5.2	41.1	10.4	2.7	146.3	95.2	12532	1617
R1-9.1		16.3	2.1	0.5	87.8	54.9	13038	1063
R1-10.1		37.6	10.9	3.2	252.4	133.1	9345	2609
R1-11.1		49.7	26.2	8.1	436.3	161.1	8843	3838
R1-12.1		21.6	10.2	1.0	147.9	68.8	9820	1388
R1-13.1		5.9			34.5	38.4	12965	425
R1-14.1	0.3	8.0	3.2	0.9	64.7	37.7	9014	715
R1-14.2		17.0	2.7		106.8	82.7	12624	1295
R1-14.3	0.7	19.6	5.0		117.1	103.1	12704	1427
R1-15.1		6.0	4.3	1.0	71.9	34.1	8717	676
R1-15.2		26.6	4.0		112.1	82.4	11447	1406
R1-16.1		62.1	16.6	5.7	289.9	111.0	10759	2274
R1-17.1		31.4	7.8	0.4	425.8	273.8	14452	4548
R1-17.2		15.2	4.4		237.6	182.1	13808	2640
R1-18.1		48.8	4.3	0.8	148.9	91.1	11250	1528
R1-19.1		51.9	3.6	1.4	169.4	99.4	11141	1738
R1-20.1		32.6	2.7	0.6	170.2	127.0	12641	1994
R1-21.1		12.2	2.7	1.1	107.7	61.6	10281	1080
R1-22.1	0.3	13.6	2.1	0.9	65.7	37.3	9380	648
R1-23.1		21.1	17.1	4.1	273.1	108.7	8864	2537
R1-24.1	28.9	150.7	83.5	18.0	685.3	226.5	11857	5487
R2-1.1		21.2	7.4	1.9	139.6	62.7	10639	1252
R2-1.2		22.9	19.7	3.2	258.6	107.0	9799	2294
R2-1.3		26.7	4.4	0.4	154.5	124.0	13265	1821
R2-2.1		25.6	10.4	4.3	234.3	99.9	10025	2197
R2-3.1	5.6	58.8	12.9	3.4	254.4	123.1	11299	2356

R2-3.2	0.5	39.2	7.8	1.2	142.7	66.7	9962	1311
R2-4.1		11.2	5.9	0.9	103.8	45.8	9644	884
R2-5.1		7.7	2.6	0.7	31.8	33.2	12549	366
R2-5.2	0.8	29.9	2.4	0.4	197.5	154.6	13947	2237
R2-5.3	15.2	63.3	13.3	2.9	291.7	167.9	12820	2984
R2-6.1	81.4	244.3	53.0	3.8	157.3	66.6	12059	1343
R2-6.2	20.5	77.6	44.3	5.5	335.5	121.9	10170	2832
R2-7.1		23.3	15.1	5.6	272.1	113.4	8898	2549
R2-7.2		40.7	4.3	1.3	123.4	76.8	11412	1294
R2-8.1		18.3	5.3	1.4	117.7	58.9	10054	1154
R2-9.1		10.7	2.6	1.7	73.4	39.7	8863	781
R2-9.2	1.1	22.6	2.3		132.0	96.3	12874	1530
RA09-CH2 Leatherwood Granite orthogneiss								
R1-1.1C		13.5	19.8	3.3	201.3	73.0	9558	1607
R1-1.2R		28.3	2.3		109.1	79.0	12964	1198
R1-2.1C	0.5	13.6	9.8	2.8	158.0	59.9	9341	1281
R1-2.2R	3.0	40.2	10.6	0.4	113.8	68.5	13076	1132
R1-3.1R		39.1	5.2	1.3	152.6	83.3	11256	1374
R1-3.2C		28.4	15.3	6.3	354.7	144.9	10005	3048
R1-4.1R	0.4	13.8	3.5	1.1	101.4	53.3	10432	896
R1-4.2R		16.9	3.8	1.9	114.5	52.9	10075	987
R1-5.1C	1.0	31.2	9.4	2.1	200.9	91.2	10875	1858
R1-5.2R		73.4	5.2	0.8	209.8	136.3	12223	2223
R1-6.1C	13.9	98.3	41.2	9.8	537.6	290.4	14622	5348
R1-6.2R	9.0	65.4	31.4	4.6	309.9	222.3	18149	3033
R1-7.1R		26.8	2.6		80.2	51.2	11720	781
R1-8.1R		17.6	4.9		306.5	289.9	16499	3613
R1-8.2C		17.0	13.5	2.1	225.3	83.9	9879	1904
R1-8.3R		17.8	7.0		229.6	196.2	15053	2689
R1-9.1C	2.8	38.0	19.2	5.2	268.8	117.2	10900	2376
R1-9.2R		18.8	9.5	1.9	143.5	91.0	10895	1495
R1-10.1R		18.2	4.1		153.9	108.6	14886	1549
R1-10.2R		17.6	3.1	0.8	185.4	184.0	15940	2269
R1-10.3C	1.9	27.7	7.8	0.8	96.4	48.7	10765	983
R1-10.4R		19.3	1.8		191.7	168.7	14342	2180
R1-10.5R	8.5	72.4	25.8	4.6	314.9	197.9	14978	3027
R1-11.1R	10.3	55.4	18.8	8.8	672.2	587.8	19718	7724
R1-12.1C		18.9	2.1		94.1	70.9	12789	1005
R1-12.2R	1.3	26.2	3.9	0.9	94.3	73.8	13323	1081
R1-13.1R	2.5	64.3	18.1	4.3	214.9	127.0	12998	2115
R1-13.2C		18.0	13.6	0.5	232.5	105.5	12870	2086
R1-13.3R		82.4	8.6	1.8	320.4	208.1	13201	3367
R1-14.1R		17.2	3.9	1.6	97.9	56.2	10251	1002
R1-15.1C		21.9	4.4	0.6	324.2	204.9	17454	3409
R1-15.2C		24.2	7.2		478.8	276.5	17008	4830

R1-15.3R		16.6	4.3		251.2	207.6	16435	2777
R1-16.1R		43.9	8.5	0.4	352.3	217.8	13133	3603
R1-17.1R		33.4	7.8		115.4	69.2	11892	1168
R1-18.1R		19.3	5.1	1.7	127.2	61.5	9603	1107
R1-19.1C		23.5	8.4	0.7	391.9	268.8	13757	4229
R1-20.1R		32.6	4.0		122.3	77.2	12006	1266
R1-21.1R		22.9	3.9	0.5	79.9	47.5	11495	822
R1-22.1R	396.5	852.0	82.7	5.8	188.7	97.9	13813	1618
R1-23.1R	0.3	14.6	7.7		427.4	390.6	18687	4868
R2-1.1R		7.9	3.7	0.9	76.3	40.8	9382	720
R2-2.1C		6.5	10.8		178.0	68.2	10844	1644
R2-3.1C		13.0	2.9	0.4	71.3	64.9	13930	816
R2-4.1C	0.8	99.8	14.7	2.9	438.8	242.5	12885	4217
R2-4.2C		98.3	10.2	1.9	352.4	214.8	12254	3540
R2-5.1C	61.0	227.3	70.0	8.1	287.6	101.8	10600	2262
R2-5.2R		16.5	4.2	2.2	122.7	63.5	9774	1032
R2-6.1R		31.6	9.2	1.5	186.2	106.8	10773	1908
R2-6.2C		22.9	9.3	2.2	217.9	103.7	10677	2096
R2-7.1C		6.7	7.7	3.2	124.9	50.7	8622	1107
R2-7.2R		27.3	4.2	0.5	122.1	75.3	11765	1316
R2-8.1R		9.4	6.9	4.7	158.3	67.0	9707	1313
R2-8.2C		18.0	21.3	6.9	267.4	85.9	9196	2171
R2-9.1R		20.4	6.2	1.7	112.2	63.2	9973	1243
R2-9.2C	0.5	40.2	11.0	2.8	258.3	108.0	10605	2191
R2-9.3R		34.1	3.8	0.7	136.3	80.3	10928	1315
R2-10.1R		26.2	4.4		157.4	105.3	12176	1583
SPG-223 Leatherwood Granite orthogneiss								
1.1		31.7	3.5		85.4	60.9	11583	927
2.1	13.5	233.0	59.6	10.7	919.3	372.0	8935	8448
2.2		27.5	1.7		81.3	69.7	11513	999
2.3	0.5	14.3			36.7	34.2	13650	434
3.1		17.0	1.3		72.9	60.9	12096	874
4.1	1.1	40.8	4.9	0.6	86.1	63.5	11361	1012
5.1	0.5	29.8	3.9	0.6	72.6	56.7	11365	856
6.1	9.4	150.5	22.5	2.4	146.6	97.4	11470	1617
7.1		29.6	2.3	0.3	78.5	54.4	11397	898
8.1		63.0	13.7	1.6	298.8	155.1	11243	3058
8.2		37.8	3.3	0.5	102.4	73.3	11696	1163
9.1		34.1	4.0		100.6	69.6	11913	1126
10.1		47.3	4.4	1.1	109.2	93.5	10398	1399
11.1	9.4	173.6	35.0	6.3	627.9	250.7	9476	5731
12.1		26.9	2.7	0.5	67.6	48.6	11386	720
13.1	1.6	36.5	10.3	1.4	95.6	72.1	13601	1098
14.1	13.8	89.7	17.3	2.5	136.1	81.3	11388	1349
15.1	2.2	34.3	3.3	0.8	86.6	70.5	13097	1019

15.2	9.2	109.1	20.6	3.7	240.6	211.9	9594	2914
15.3		4.7			5.0	23.2	14576	127
16.1	35.0	129.4	29.5	6.5	90.7	61.2	11485	990
17.1	72.5	342.1	116.8	41.2	273.4	163.7	11144	2885
18.1		39.9	3.1	0.5	112.2	80.6	11739	1311
19.1	0.8	45.0	3.7	0.7	99.6	67.3	10931	1073
20.1	4.6	53.0	12.3	2.4	91.5	57.5	10935	912
20.2	0.3	35.3	3.7	0.6	147.3	117.6	11663	1791
20.3	16.8	106.8	19.8	4.8	135.7	83.6	11128	1474
21.1	4.1	44.7	5.7	1.4	70.0	49.5	11473	769
22.1	0.3	102.2	21.2	6.4	407.3	191.3	6909	4163
23.1	1.0	27.4	4.4	1.3	79.7	59.5	13207	824
23.2	3.2	34.8	5.7	0.4	193.3	142.2	14505	2187
23.3	6.5	57.9	9.7	2.2	110.4	69.6	11943	1110
24.1		36.5	2.8		90.1	62.7	11416	942
25.1		15.0	1.6	0.5	43.6	46.1	13140	493
26.1		34.4	4.4	0.4	97.8	65.0	11712	993
27.1	3.2	49.2	7.0	1.7	119.2	77.9	12289	1185
28.1		35.8	3.7		91.6	68.5	12637	994
29.1		32.0	2.2	0.4	101.4	74.3	12763	1067
30.1		31.7	2.7	0.5	75.0	45.6	11631	701
31.1	1.0	53.3	7.3	0.8	188.4	119.8	12423	1915
32.1		36.2	3.8	0.3	145.7	93.4	11269	1648
33.1	0.1	9.3	12.4	3.3	143.6	51.7	9233	1230
34.1	9.3	64.6	14.1	3.8	130.3	75.5	10354	1357
34.2	3.6	49.5	10.0	2.7	82.8	57.3	10697	915

Notes: All reported values are normalized to chondrite using the values of Anders and Grevesse (1989) modified by Korotev (1996).

[1] Empty cells represent a concentration below detection limits.